



1 **Relative Importance of High-Latitude Local and Long-Range**
2 **Transported Dust to Arctic Ice Nucleating Particles and**
3 **Impacts on Arctic Mixed-Phase Clouds**

4 Yang Shi¹, Xiaohong Liu¹, Mingxuan Wu², Ziming Ke¹, and Hunter Brown¹

5 ¹Department of Atmospheric Sciences, Texas A&M University, College Station, TX, USA

6 ²Atmospheric Sciences and Global Change Division, Pacific Northwest National Laboratory,
7 Richland, WA, USA

8

9 *Correspondence to:* Xiaohong Liu (xiaohong.liu@tamu.edu)

10



11 **Abstract.** Dust particles, serving as ice nucleating particles (INPs), may impact the Arctic
12 surface energy budget and regional climate by modulating the mixed-phase cloud properties and
13 lifetime. In addition to long-range transport from low latitude deserts, dust particles in the Arctic
14 can originate from local sources. However, the importance of high latitude dust (HLD) as a
15 source of Arctic INPs (compared to low latitude dust (LLD)) and its effects on Arctic mixed-
16 phase clouds are overlooked. In this study, we evaluate the contribution to Arctic dust loading
17 and INP population from HLD and six LLD source regions by implementing a source-tagging
18 technique for dust aerosols in version 1 of the US Department of Energy's Energy Exascale
19 Earth System Model (E3SMv1). Our results show that HLD is responsible for 30.7% of the total
20 dust burden in the Arctic, whereas LLD from Asia and North Africa contribute 44.2% and
21 24.2%, respectively. Due to its limited vertical transport as a result of stable boundary layers,
22 HLD contributes more in the lower troposphere, especially in boreal summer and autumn when
23 the HLD emissions are stronger. LLD from North Africa and East Asia dominates the dust
24 loading in the upper troposphere with peak contributions in boreal spring and winter. The
25 modeled INP concentrations show a better agreement with both ground and aircraft INP
26 measurements in the Arctic when including HLD INPs. The HLD INPs are found to induce a net
27 cooling effect (-0.24 W m^{-2} above 60°N) on the Arctic surface downwelling radiative flux by
28 changing the cloud phase of the Arctic mixed-phase clouds. The magnitude of this cooling is
29 larger than those induced by North African and East Asian dust (0.08 and -0.06 W m^{-2} ,
30 respectively), mainly due to different seasonalities of HLD and LLD. Uncertainties of this study
31 are discussed, which highlights the importance of further constraining the HLD emissions.

32



33 **1 Introduction**

34 The Arctic has experienced long-term climate changes, including rapid warming and shrinking
35 in sea ice extent. Arctic mixed-phase clouds (AMPCs), which occur frequently throughout the
36 year, strongly impact the surface and atmospheric energy budget and are one of the main
37 components driving the Arctic climate (Morrison et al., 2012; Shupe and Intrieri, 2004; Tan and
38 Storelvmo, 2019). The AMPCs lifetime, properties, and radiative effects are closely connected to
39 the primary ice formation process, as the formed ice crystals grow at the expense of cloud liquid
40 droplets through the Wegener-Bergeron-Findeisen (WBF) process (Liu et al., 2011; M. Zhang et
41 al., 2019). Large ice crystals with higher fall speeds than liquid droplets can readily initiate
42 precipitation and further deplete cloud liquid through the riming process.

43 Primary ice formation in mixed-phase clouds only occurs heterogeneously with the aid of ice
44 nucleating particles (INPs). According to Vali et al. (1985), the heterogeneous ice nucleation is
45 classified into four different modes: through the collision of an INP particle with supercool liquid
46 droplet (contact freezing), by an INP particle immersed in a liquid droplet (immersion freezing),
47 when the INP particle also serves as a cloud condensation nucleus (condensation freezing), or by
48 the direct deposition of water vapor to a dry INP particle (deposition nucleation). The immersion
49 freezing is usually treated together with condensation freezing in models, as instruments cannot
50 distinguish between them (Vali et al., 2015). This immersion/condensation freezing is generally
51 thought to be the most important ice nucleation mode in the mixed-phase clouds (de Boer et al.,
52 2011; Prenni et al., 2009; Westbrook and Illingworth, 2013). It remains a significant challenge to
53 characterize the INP types and concentrations, partially because only a very small fraction of
54 aerosols can serve as INPs (DeMott et al., 2010). This is especially the case for the clean



55 environment in the Arctic. Therefore, the potential sources and amounts of Arctic INPs are still
56 largely unknown.

57 Mineral dust aerosols are identified as one of the most important types of INPs in the
58 atmosphere due to their high ice nucleation efficiency (DeMott et al., 2003; Hoose and Möhler,
59 2012; Murray et al., 2012; Atkinson et al., 2013) and their abundance in the atmosphere (Kinne
60 et al., 2006). They are mainly emitted from arid and semi-arid regions located at low- to mid-
61 latitudes, such as North Africa, the Middle East, and Asia. Observational studies found that LLD
62 can be transported to the Arctic (Bory et al., 2003; VanCuren et al., 2012; Huang et al., 2015)
63 and act as a key contributor to the Arctic INP population (Si et al., 2019). A modelling study also
64 suggested that low latitude dust (LLD) has a large contribution to dust concentrations in the
65 upper troposphere of the Arctic (Groot Zwaafink et al., 2016), since LLD is usually lifted by
66 convection and topography and then transported poleward following slantwise isentropes. This
67 finding confirms the potential of LLD to serve as INPs in AMPCs. The impact of LLD INPs on
68 clouds was further investigated by Shi and Liu (2019), who found that LLD INPs induce a net
69 cooling cloud radiative effect in the Arctic, due to their impacts on cloud water path and cloud
70 fraction.

71 Although LLD has attracted much of the attention in the past, it is recognized that 2–3% of the
72 global dust emission is produced by local Arctic sources above 50°N (Bullard et al., 2016),
73 which include Iceland (Arnalds et al., 2016; Dagsson-Waldhauserova et al., 2014; Prospero et al.,
74 2012), Svalbard (Dörnbrack et al., 2010), Alaska (Crusius et al., 2011), and Greenland (Bullard
75 and Austin, 2011). Groot Zwaafink et al. (2016) found that high latitude dust (HLD) contributes
76 27% of the total dust burden in the Arctic. Different from LLD, most of the emitted HLD is



77 restricted at the lower altitudes in the Arctic, because of the stratified atmosphere in the cold
78 environment (Bullard, 2017; Groot Zwaafink et al., 2016).

79 It is also noted that HLD is likely an important source to the observed INPs in the Arctic,
80 especially during the warm seasons. For example, Irish et al. (2019) suggested that mineral dust
81 from Arctic bare lands (likely eastern Greenland or north-western continental Canada) is an
82 important contributor to the INP population in the Canadian Arctic marine boundary layer during
83 summer 2014. Attempts have been made to quantify the ice nucleating ability of HLD.
84 Paramonov et al. (2018) found that the Icelandic glaciogenic silt had a similar ice nucleating
85 ability as LLD at temperatures below $-30\text{ }^{\circ}\text{C}$. Similarly, Sanchez-Marroquin et al. (2020)
86 suggested that the ice nucleating ability of aircraft-collected Icelandic dust samples is slightly
87 lower but comparable with that of the LLD. Some other studies also noticed that HLD can act as
88 efficient INPs at warm temperatures. As early as the 1950s, the airborne dry dust particles from
89 permafrost ground at Thule, Greenland, were found to nucleate ice at temperatures as warm as -5
90 $^{\circ}\text{C}$ (Fenn and Weickmann, 1959). This is corroborated by a more recent study which investigated
91 the glacial outwash sediments in Svalbard and ascribed the remarkably high ice nucleating
92 ability to the presence of soil organic matter (Tobo et al., 2019).

93 Despite their potential importance, HLD sources are largely underestimated or even omitted in
94 global models (Zender et al., 2003). Fan (2013) noticed that the autumn peak in measured dust
95 concentrations at Alert was underestimated by the model, likely due to a lack of local dust
96 emission. Similarly, Shi and Liu (2019) also mentioned that the distinction of simulated and
97 satellite retrieved dust vertical extinction in the Arctic became larger near the surface.

98 In this study, we account for the HLD dust emission by replacing the default dust emission
99 scheme (Zender et al., 2003) with the Kok et al. (2014a, b) scheme in the Energy Exascale Earth



100 System Model version 1 (E3SMv1). We further track explicitly the dust aerosols emitted from
101 the Arctic (HLD) and six major LLD sources using a newly developed source-tagging technique
102 in E3SMv1. The objectives of this study are to (1) examine the source attribution of the Arctic
103 dust aerosols in the planetary boundary layer and in the free troposphere; (2) examine the
104 contribution of dust from various sources to the Arctic dust INPs; and (3) quantify the
105 subsequent influence of dust INPs from various sources on the Arctic mixed-phase cloud
106 radiative effects. We are particularly interested in the relative importance of local HLD versus
107 long-range transported LLD.

108 The paper is organized as follows. The E3SMv1 model and experiments setup are introduced
109 in Section 2. Section 3 presents model results and comparisons with observations. The
110 uncertainties are discussed in Section 4, and Section 5 summarizes the results.

111 **2 Methods**

112 **2.1 Model description and experiment setup**

113 Experiments in this study are performed using the atmosphere component (EAMv1) of the U.S.
114 Department of Energy (DOE) E3SMv1 model (Rasch et al., 2019). The model predicts number
115 and mass mixing ratios of seven aerosol species (i.e., mineral dust, black carbon (BC), primary
116 organic aerosol, secondary organic aerosol, sulfate, sea salt, and marine organic aerosol (MOA))
117 through a four-mode version of modal aerosol module (MAM4) (Liu et al., 2016; Wang et al.,
118 2020). The four aerosol modes are Aitken, accumulation, coarse, and primary-carbon modes,
119 while dust aerosols are carried in accumulation and coarse modes. Aerosol optical properties in
120 each mode is parameterized following Ghan and Zaveri (2007). The dust optics used in this study
121 are updated according to Albani et al. (2014).



122 EAMv1 includes a two-moment stratiform cloud microphysics scheme (MG2) (Gettelman and
123 Morrison, 2015), with the heterogenous ice nucleation in mixed-phase clouds following the
124 classical nucleation theory (CNT) (Y. Wang et al., 2014). Immersion/condensation, contact, and
125 deposition nucleation on dust and BC are treated in the CNT scheme. It should be noted that the
126 WBF process rate in EAMv1 is tuned down by a factor of 10, which results in more prevalent
127 supercooled liquid water clouds in high latitudes than observations and many other global
128 climate models (Y. Zhang et al., 2019; Zhang et al., 2020). In addition, the Cloud Layers Unified
129 By Binormals (CLUBB) parameterization (Bogenschutz et al., 2013; Golaz and Larson, 2002;
130 Larson et al., 2002) is used to unify the treatments of planetary boundary layer turbulence,
131 shallow convection, and cloud macrophysics. Deep convection is treated by the Zhang and
132 McFarlane (1995) scheme.

133 The experiments we conducted for this study is shown in Table 1. For the control experiment
134 (hereafter CTRL), the EAMv1 was integrated from July 2006 to the end of 2011 at 1° horizontal
135 resolution and 72 vertical layers. The first six months of the experiment were treated as model
136 spin-up and the last five-year results were used in analyses. The horizontal wind components
137 were nudged to the MERRA2 meteorology with a relaxation timescale of 6 hour (Zhang et al.,
138 2014). In addition to CTRL, we conducted three sensitivity experiments to investigate the INP
139 effect of dust from major source regions. In these sensitivity experiments, heterogeneous ice
140 nucleation in the mixed-phase clouds by dust from local Arctic sources, North Africa, and East
141 Asia is turned off (i.e., noArc, noNAf, and noEAs, respectively). The other settings of these
142 three experiments are identical to CTRL. Analyses related to the sensitivity experiments are
143 provided in Section 3.4.

144



145 2.2 Dust emission parameterization and source-tagging technique

146 Dust emission in the default EAMv1 is parameterized following Zender et al. (2003) (Z03),
147 which uses semi-empirical dust source functions to address the spatial variability in soil
148 erodibility. The HLD emission is omitted in the Z03 scheme, since it was thought to be dubious
149 (Zender et al., 2003). In this study, we replaced the Z03 scheme with another dust emission
150 parameterization (Kok et al., 2014a, b) (K14) that avoids using a source function. The K14
151 scheme is able to produce the HLD emission over Iceland, the Greenland coast, Canada,
152 Svalbard, and North Eurasia (Figure 1a). Furthermore, to address the overestimation in dust
153 emission in clay size ($< 2 \mu\text{m}$ diameter) (Kok et al., 2017), we changed the size distribution of
154 emitted dust particles from Z03 to that based on the brittle fragmentation theory (Kok, 2011). 1.1%
155 of the total dust mass is emitted to the accumulation mode and 98.9% of that is emitted to the
156 coarse mode based on the brittle fragmentation theory, whereas the fractions are 3.2% and 96.8%,
157 respectively in Z03.

158 To quantify the source attribution of dust, we implemented a dust source-tagging technique in
159 EAMv1. This modeling tool was previously applied to BC (H. Wang et al., 2014; Yang et al.,
160 2017b), sulfate (Yang et al., 2017a), and primary organic aerosol (Yang et al., 2018) in the
161 Community Atmosphere Model version 5 (CAM5). With this method, dust originating from
162 different sources can be tracked explicitly in a single model experiment. As shown in Figure 1a,
163 dust emissions from 7 source regions are tagged: Arctic (Arc; above 60°N , HLD source), North
164 America (NA_m), North Africa (NA_f), Central Asia (CA_s), Middle East and South Asia (MSA),
165 East Asia (EA_s), and rest of the world (RoW). The Arctic source is further divided into four sub-
166 sources: Alaska (Ala), North Canada (NCa), Greenland and Iceland (GrI), and North Eurasia
167 (NEu) (Figure S1), which are used in the analysis of INP sources in Section 3.3. RoW represents



168 the three major dust sources in the Southern Hemisphere (South America, South Africa, and
169 Australia), along with very low emissions from Europe and the Antarctic.

170 The global dust emission for CTRL is 5640 Tg yr^{-1} , which is tuned so that the global average
171 dust aerosol optical depth (DOD) is 0.031. This is within the range of the observational estimate
172 (0.030 ± 0.005) by Ridley et al. (2016). To maintain the magnitude of the global averaged DOD,
173 our tuned global dust emission exceeds the range of the AeroCom (Aerosol Comparisons
174 between Observations and Models) models (500 to 4400 Tg yr^{-1} ; Huneeus et al., 2011), likely
175 due to a short lifetime caused by too strong dust dry deposition at the bottom layer near the dust
176 source regions in EAMv1 (Wu et al., 2020). It is also about 2000 Tg yr^{-1} higher than the previous
177 EAMv1 studies (Shi and Liu, 2019; Wu et al., 2020), because we distribute less dust mass into
178 the accumulation mode and more dust mass into the coarse mode based on Kok (2011). The
179 HLD emission is further tuned up by 10 times so that it accounts for 2.6% (144 Tg yr^{-1}) of the
180 global dust emission (Figure 1b), which is comparable with the recent estimates of 2-3% above
181 50°N by Bullard et al. (2016) and of 3% above 60°N by Groot Zwaafink et al. (2016). The
182 majority of global dust emission is contributed from North Africa (51.9%, 2929 Tg yr^{-1}) and
183 Asia (37.7%, 2124 Tg yr^{-1}), with Asian emissions composed of MSA (20.2%, 1140 Tg yr^{-1}), EAs
184 (10.9%, 613 Tg yr^{-1}), and CAs (6.6%, 371 Tg yr^{-1}). NAM has a weak dust emission of 33.4 Tg
185 yr^{-1} that only contributes 0.6% to the global emission, while the RoW has a combined
186 contribution of 7.3% (410 Tg yr^{-1}). In addition, the seasonal variations between HLD and LLD
187 emissions are different - the HLD (Arctic) source is more active in late summer and autumn,
188 while the LLD sources (e.g., NAF, MSA, EAs) peak in spring and early summer (Figure 1c).



189 **3 Result**

190 **3.1 Model validation**

191 To evaluate the model performance in simulating the dust cycle, we compare the model
192 predictions with measured aerosol optical depth (AOD), dust surface concentrations, and dust
193 deposition fluxes from global observation networks (Figure 2). We select and process the level
194 2.0 AOD data at 40 “dust-dominated” Aerosol Robotic NETwork (AERONET; Holben et al.,
195 1998) stations following Kok et al. (2014b). For dust surface concentrations, we use the same
196 measurements at 22 sites, which Huneus et al. (2011) used for the AeroCom comparison, and
197 further extend the dataset with measurements at three high latitude stations: Heimaey (Prospero
198 et al., 2012), Alert (Fan, 2013), and Trapper Creek (Interagency Monitoring of Protected Visual
199 Environments; IMPROVE). It is noted that the measurements at Trapper Creek only include dust
200 particles smaller than $2.5 \mu\text{m}$ and are only compared with simulated dust concentrations at the
201 same size range. All other concentration measurements capture dust particles below $40 \mu\text{m}$ and
202 are compared with simulated dust over the whole size range ($< 10 \mu\text{m}$). The dust deposition
203 fluxes dataset, which including 84 stations, is also the same as Huneus et al. (2011). The
204 locations of the observation network are shown in Figure 2d, with the AOD data taken close to
205 source regions and the dust surface concentrations and deposition fluxes measured at relatively
206 remote regions. The Pearson correlation coefficient (r) are provided for each comparison.

207 In general, the three comparisons indicate that our CTRL simulation is capable of capturing
208 the global dust cycle in both near the source and remote regions. As shown in Figure 2a, the
209 modeled AOD is within a factor of two of the observations over most of the stations. The
210 correlation of the AOD comparison is 0.73, which is comparable to the best performing
211 simulation ($r = 0.72$) in Kok et al. (2014b). Our model also does a fairly good job in simulating



212 the dust surface concentrations (Figure 2b) and produces a correlation coefficient of 0.83. For the
213 three high latitude sites, the model shows moderate underestimation at Heimaey and Trapper
214 Creek, but large positive bias at Alert (see discussion below). The correlation coefficient for
215 simulated dust deposition fluxes is also within the range of the AeroCom comparisons (0.08 to
216 0.84) in Huneus et al. (2011). The model results over most of the sites are within one order of
217 magnitude difference, except at the polar regions. In particular, the model overestimates the dust
218 deposition flux in Greenland (red triangles in Figure 2c and 2d) by around two orders of
219 magnitude, likely due to too strong local emissions simulated near the coast of Greenland (Figure
220 1a).

221 The seasonal cycle of dust surface concentrations at the three Arctic stations (Heimaey, Alert,
222 and Trapper Creek) are shown in Figure 3, along with the contribution from seven tagged
223 sources. The simulated dust concentrations at Heimaey are dominated by HLD and agree well
224 with the observation in late summer and autumn (Figure 3a). Its annual-averaged low bias shown
225 in Figure 2b mainly comes from the springtime, when Prospero et al. (2012) found the observed
226 dust are related to dust storms in Iceland, indicating a possible underestimation in the simulated
227 Icelandic dust during this time. The HLD also dominates the surface dust concentrations at Alert
228 (Figure 3b), leading to a significant overestimation from June to September in our simulation,
229 which possibly implies a high bias and wrong seasonal cycle of HLD emission over Greenland
230 and North Canada. The Trapper Creek station is instead dominated by LLD from East Asia and
231 shows an underestimation for most of the year. It is noted that we only include fine dust
232 (diameter $< 2.5 \mu\text{m}$) for the comparison at Trapper Creek. Larger size range is likely to be more
233 influenced by HLD sources. The low bias here, especially that during the autumn, can be related
234 to the missing of local emissions from the coast of Southern Alaska (Figure 1a) that occurs most



235 frequently in autumn (Crusius et al., 2011). An underestimation of the transport from Saharan
236 dust may also contribute slightly, as the influence from Saharan dust is found during mid-May at
237 Trapper Creek (Breider et al., 2014).

238 The simulated Arctic dust vertical profiles are also compared with the measured dust
239 concentrations during the Arctic Research of the Composition of the Troposphere from Aircraft
240 and Satellites (ARCTAS) flight campaign (Figure 4) (Jacob et al., 2010). The ARCTAS
241 campaign was conducted over the North American Arctic in April and July 2008. The simulated
242 profiles are averaged over the regions where the aircraft flew, in accordance with Groot
243 Zwaafink et al. (2016). In April, the model does a good job in capturing the Arctic dust vertical
244 profiles (Figure 4a). However, in July, the model underestimates dust by a factor of 2 to 5
245 between 3 and 10 km (Figure 4b). It also shows an overestimation near the surface in July, which
246 agrees with the surface concentrations comparison at Alert station (Figure 3b). The
247 underestimation in the upper troposphere and overestimation near the surface likely imply a too
248 weak vertical transport of HLD in the North American Arctic in summertime. The high bias in
249 the upper troposphere may also be related to an underrepresentation of LLD transport.

250 Finally, we evaluate the simulated dust extinction against the Cloud-Aerosol Lidar and
251 Infrared Pathfinder Satellite Observation (CALIPSO) retrieval (Luo et al., 2015b, a), which
252 includes nighttime dust extinction for the period of 2007 to 2009. To make an apple-to-apple
253 comparison, the modeled dust extinction is sampled along the CALIPSO tracks and screened by
254 cloud fraction (Wu et al., 2020). For this comparison, we only use the first three years (2007 to
255 2009) of the CTRL simulation to be consistent with the observation period. Overall, the model
256 does a good job in capturing the Arctic dust extinction vertical profiles (Figure 5). We notice that
257 the simulated dust extinction is lower than CALIPSO retrievals at the upper troposphere in



258 summer, which agrees with the ARCTAS comparisons. Moreover, the HLD has a large
259 contribution in the lower troposphere in boreal summer and autumn, which is consistent with its
260 strong emission at that time. In contrast, LLD plays a more dominant role in the upper
261 troposphere, where African dust contributes the most in the springtime and East Asian dust has a
262 larger contribution in the other seasons.

263 **3.2 Arctic dust mass source attribution**

264 Table 2 summarizes the relative contributions from individual sources to the total Arctic dust
265 burden, while the transport pathways can be identified from the dust burden spatial distribution
266 for each source in Figure 6. We also calculate the regional burden efficiency for each source
267 (Table S1), which is defined as the mean contribution to the Arctic dust column burden divided
268 by the corresponding dust emission (H. Wang et al., 2014). This metric represents the sensitivity
269 of Arctic dust loading to per unit change of dust emission from each source (i.e., the poleward
270 transport efficiency of each source).

271 Our model results suggest that the HLD (Arc) is the largest contributor (30.7%) to the annual
272 mean Arctic dust burden among all the tagged sources. As shown in Figure 6a, the local dust is
273 confined within the high latitudes, with the higher amounts near the sources in North Canada,
274 coast of Greenland, and Iceland. The interior of the Greenland ice sheet, with its higher
275 elevations, is more influenced by LLD from Asia and North Africa than HLD. This is due to the
276 suppression of vertical transport of local emissions by the stratified atmosphere as well as limited
277 convection in the Arctic (Baddock et al., 2017; Bullard et al., 2016).

278 On the other hand, all LLD sources are responsible for 69.3% of the dust loading in the Arctic,
279 with considerable contributions from North Africa (24.2%) and Asia (in total 44.2%; EAs:
280 19.9%, MSA: 11.5%, CAs: 12.8%), and minor contributions from NAm (0.1%) and RoW (nearly



281 0). The North African dust is primarily transported westward to the Atlantic and southward to
282 Sahel, with a smaller fraction transported directly northward or northeastward across the Eurasia
283 to the Arctic (Figure 6c; Shao et al., 2011). The westward trajectory can also bring dust to the
284 Arctic through the Azores high (e.g., VauCuren et al., 2012), but this pathway is not clearly seen
285 on Figure 6c likely due to the strong wet removal process over the North Atlantic. As evident by
286 the low transport efficiency in Table S1, the significant contribution of the North African dust to
287 the Arctic dust burden is mainly due to its massive emission. However, this is not the case for
288 EAs. The East Asian dust is first lifted vertically by topography and convection (Shao et al.,
289 2011) and is widely spread over the Northern Hemisphere mid- and high-latitude regions through
290 the westerly flow in the upper troposphere (Figure 6f). The high elevation of East Asian dust
291 plumes results in weaker removal processes and thus an efficient poleward transport. As shown
292 in Table S1, the annual transport efficiency of the East Asian dust is relatively high among the
293 LLD sources, which is nearly three times larger than that of the North African dust. The
294 poleward transport of dust from CAs and MSA both takes the pathway across Siberia (Figure 6d
295 and 6e). The transport efficiency of the CAs dust is two times higher than that of the MSA dust
296 (Table S1). This is attributed to CAs being closer to the Arctic and having less southward dust
297 transport than MSA. The impact of NAM dust is limited by its weak emission (Figure 6b), while
298 dust emitted in the Southern Hemisphere (RoW) can hardly pass the equator (Figure 6g).

299 Earlier modeling studies (Breider et al., 2014; Groot Zwaafink et al., 2016; Luo et al., 2003;
300 Tanaka and Chiba, 2006) also quantify the relative contributions of dust from various regions to
301 the Arctic dust loading. Among these studies, only Groot Zwaafink et al. (2016) includes HLD.
302 Our estimate about the HLD percent contribution is close to that from their study (27%). For
303 LLD, our conclusion about the dominant role of African and Asian dust to the Arctic dust burden



304 is also corroborated by these previous studies. However, the relative importance of African and
305 Asian dust is uncertain. Based on our results, the Asian dust is responsible for 65% of the LLD
306 transport to the Arctic, while the African dust only contributes 35%. Other studies find that 50%
307 (Groot Zwaaftink et al., 2016; Luo et al., 2003; Tanaka and Chiba, 2006) to as much as 65%
308 (Breider et al., 2014) of the LLD in the Arctic is attributed to North Africa. These discrepancies
309 may be explained by the different dust emission and scavenging, dust size distribution,
310 meteorological fields, and/or time periods for the model simulation. For example, North Africa
311 dust in our study contributes slightly less (51.9%) to the global dust emission than the other
312 studies (from 57% to 67%). Isotopic analysis (Bory et al., 2002, 2003) and case studies (Huang
313 et al., 2015; Stone et al., 2005; VanCuren et al., 2012) have proved that both Asian and African
314 dust can be transported to the Arctic. However, it remains unclear which of them contributes
315 more to the Arctic dust loading due to the limited observational constraints.

316 HLD and LLD source regions also have very distinct vertical distributions in the Arctic.
317 Figures 7a and 7b show the annual mean vertical profiles of Arctic dust concentrations from
318 various sources and their percentage contributions, respectively. The Arctic dust in the lower
319 atmosphere is dominated by the local source. HLD accounts for more than 30% of the Arctic
320 dust concentrations below 800 hPa, with up to 85% contribution near the surface. However, due
321 to the weak vertical transport, the HLD contribution decreases rapidly with height and is less
322 than 10% above 700 hPa. In contrast, LLD has a higher contribution in the mid- and upper
323 troposphere than near the surface. Such a vertical distribution of LLD is consistent with Stohl
324 (2006) and Groot Zwaaftink et al. (2016). As Stohl (2006) found, aerosols originating from the
325 warm subtropics are transported poleward following the uplifted isentropes and the Arctic lower
326 atmosphere is dominated by the near-impenetrable cold polar dome. Therefore, there is a



327 slantwise lifting of low latitude aerosols during their poleward transport. NAF and EAs are the
328 two key contributors to the Arctic dust vertical concentrations, each of which contributes up to
329 one third of the total dust concentrations above 700 hPa. Dust emission from MSA also has a
330 moderate contribution (15-20%) that increases gradually with height, while the contribution from
331 CAs peaks at 700 to 800 hPa, indicating a lower altitude transport pathway than the EAs and
332 MSA dust.

333 In addition, the Arctic dust undergoes a strong seasonal cycle (Table 2 and Figure 7c-j).
334 Because of the strong local emissions (Figure 1c), about half of the Arctic dust burden in
335 summer and autumn come from HLD, with more than 50% contribution of Arctic dust
336 concentrations below 850 hPa in these two seasons. In contrast, LLD plays a dominant role in
337 spring and winter. The North African dust has the largest contribution in spring, which accounts
338 for about 45% of the total dust concentrations above 700 hPa. The East Asian dust is more
339 important in the other three seasons. Due to its high emission height, the relative contribution
340 from EAs tends to increase with height and reaches 30% to 50% of the total dust concentration
341 above 500 hPa in summer, spring, and winter.

342 **3.3 Immersion freezing on dust in the AMPCs**

343 We are particularly interested in the contribution of various dust sources to the Arctic INP
344 populations. Therefore, we compare the simulated INP concentrations with nine Arctic field
345 measurements, which are summarized in Table 3. The modeled dust INP concentrations are
346 diagnosed from monthly averaged aerosol properties using two ice nucleation parameterizations,
347 DeMott et al. (2015; hereafter as D15) and Sanchez-Marroquin et al. (2020; hereafter as SM20).
348 The D15 parameterization, which is derived for the Saharan and Asian dust, relates dust INP
349 number concentrations to the number concentration of dust particles larger than 0.5 μm diameter



350 and is found to produce the most reasonable LLD INP concentrations in EAMv1 (Shi and Liu,
351 2019). It is applied to LLD only and all the dust aerosols (LLD and HLD) in Figure 8a and
352 Figure 8b, respectively. The SM20 parameterization, which is derived for the HLD Icelandic
353 dust, describes the dust INP number concentrations as a function of surface active site density
354 and total dust surface area. Considering the possibly different ice nucleation ability between
355 HLD and LLD, we only applied the SM20 parameterization to HLD and the D15
356 parameterization is still applied to LLD in Figure 8c. To account for the contributions from other
357 aerosol types, we also calculate the INP concentrations from BC (Fig. 8d) and sea spray aerosol
358 (SSA; includes MOA and sea salt) (Fig. 8e) following Schill et al. (2020; hereafter as Sc20) and
359 McCluskey et al. (2018; hereafter as M18), respectively.

360 Overall, only including LLD as INPs results in up to four orders of magnitude underprediction
361 compared to observations (Figure 8a), while taking into account the contribution from HLD
362 greatly improves the model performance by increasing the simulated dust INP concentrations
363 (Figure 8b and 8c). The two dust parameterizations agree well with each other in simulating
364 HLD INPs, with SM20 producing slightly higher results than D15. Our modeling results also
365 indicate that BC and SSA have much less contributions to INP than dust in all the nine field
366 campaigns (Figure 8d and 8e).

367 A detailed analysis of sources of the INPs for the nine datasets based on modeling analyses
368 and the corresponding observations in the literature are provided in Table 3. Modeling results
369 indicate that HLD has larger contributions to the INPs for the campaigns conducted in summer
370 and autumn than spring, in agreement with the observations. Also, ground-based measurements
371 are more influenced by the nearby HLD sources, while LLD from EAs and Naf contributes
372 more to the aircraft measurements.



373 Our modeling analyses about the INP sources agree well with the observational studies at
374 Alert in spring 2016 and near Iceland in autumn 2014 (symbol “C” and “I” in Figure 8,
375 respectively), while the model underestimates the observed INP concentrations in both cases.
376 The low bias in dataset C indicates an underprediction in the long-range transport of Asian dust
377 to the Arctic surface in springtime. The underestimation in dataset I is more likely due to the fact
378 that some of the aircraft measurements were taken inside the Icelandic dust plumes (Sanchez-
379 Marroquin et al., 2020), which cannot be resolved by the monthly mean model output and the
380 coarse model horizontal resolution (1°). Such uncertainties exist in all the model-observation
381 comparisons.

382 Some other comparisons in INP sources reveal the lack of marine and carbonaceous INPs in
383 the model. The model results show a dominance of dust INPs in spring 2017 at Zeppelin and
384 Oliktok Point (symbol “D” and “E” in Figure 8) and in Autumn 2004 at Utqiagvik (symbol “H”
385 in Figure 8), while the observational studies suggested the importance of marine sources at the
386 first two locations and of carbonaceous aerosols at Utqiagvik. Therefore, it is likely that the
387 model underestimates the contribution of MOA (Wilson et al., 2015; Zhao et al., 2021a) and
388 does not account for terrestrial biogenic INPs (Creamean et al., 2020) due to the lack of
389 treatments in the model. In addition, both D15 and SM20 schemes cannot represent the high ice
390 nucleating ability of HLD at warm temperatures at Zeppelin in summer 2016 (symbol “G” in
391 Figure 8), which is attributed to soil organic matter by Tobo et al. (2019). When these organics
392 are taken into account in the model, model overestimation for site G will get even worse,
393 implying an overestimation of surface dust concentrations and/or HLD dust emission at Svalbard
394 in the summertime. In summary, the model’s INP biases in the Arctic are likely due to biases in
395 the simulated aerosol fields (e.g., dust, MOA, and BC) and uncertainties in current ice nucleation



396 parameterizations or missing representations of other INP sources (e.g., terrestrial biogenic
397 aerosols).

398 The comparisons above are based on INP concentrations at a given temperature set by the INP
399 instruments, which reflects the potential INP populations under ambient aerosol conditions. Next,
400 we examine the immersion freezing rate of dust originating from the seven tagged sources
401 (Figure 9) to evaluate the influences of HLD and LLD on ice nucleation processes in mixed-
402 phase clouds. It is noted that the immersion freezing rate here is calculated online in the model
403 using the ambient temperature and the default CNT ice nucleation parameterization.

404 Compared with its contribution to the dust burdens, the contribution of the HLD to the annual
405 mean mixed-phase cloud immersion freezing rate is relatively small (~10% below 600 hPa)
406 (Figure 9a). This is because the HLD is mainly located in the lower troposphere and not a lot of
407 HLD can reach the mixed-phase cloud levels (or the freezing level), especially under the case
408 that the HLD tends to be more prevalent in the warm seasons (see more discussion below).
409 Among the LLD sources, North African dust (Figure 9c) and East Asian dust (Figure 9f) are the
410 two major contributors, both of which are responsible for more than 20% of the annual mean
411 immersion freezing rate in the mixed-phase clouds. Consistent with the vertical distribution of
412 dust concentrations, the North African dust has its maximum contribution (30-40%) at around
413 500 hPa, while the East Asian dust plays a more important role at higher altitudes (above 400
414 hPa). Dust from Central Asia also has a moderate contribution (~20%) to the immersion freezing
415 rate in the Arctic (Figure 9d).

416 Considering the different seasonality of HLD and LLD in the Arctic, we next investigate the
417 seasonal variations of the immersion freezing rate in the Arctic mixed-phase clouds from HLD
418 and two dominating LLD sources (NAf and EAs) (Figure 10). HLD has the largest contribution



419 to the Arctic immersion freezing rate in boreal autumn, with more than 30% below 700 hPa and
420 up to 50% near the surface (Figure 10c). It is related to the prevalence of HLD and relatively
421 cold temperatures during this time in the Arctic. This is not the case for the summer, when the
422 freezing level is relatively high. Although it is responsible for 50% of the total Arctic dust
423 burden in the boreal summer, HLD has a limited contribution to the immersion freezing rate in
424 the clouds (Figure 10b), because its weak vertical transport makes it hard to reach the freezing
425 line. The contrast results in summer and autumn suggest that the immersion freezing rate in the
426 Arctic clouds is influenced by air temperature in addition to the aerosols. It also implies that the
427 surface INP measurements may not reflect the complete picture of INP effects and more aircraft
428 INP measurements are needed in the future. The seasonal variations of the immersion freezing
429 rate from NAF and EAs are weaker than that from HLD, but are still subjected to the vertical
430 temperature change with season. The North African dust contributes more in spring and winter,
431 while the East Asian dust is more important in summer and autumn.

432 **3.4 Impact on cloud properties and radiative fluxes**

433 Dust INPs can freeze the supercooled liquid droplets, which impacts the cloud microphysical
434 and macrophysical properties and modulates the Earth's radiative balance. To examine such
435 impacts, we conduct three sensitivity experiments that turn off the heterogeneous ice nucleation
436 in the mixed-phase clouds by dust from Arctic local source, North Africa, and East Asia,
437 respectively (i.e., noArc, noNAF, and noEAs in Table 1). The impacts of dust INPs from each
438 source are determined by subtracting the respective sensitivity experiment from CTRL. Due to
439 the feedbacks in dust emission and wet scavenging caused by changing cloud properties, the dust
440 concentrations in the sensitivity experiments are not identical to CTRL, but the absolute
441 differences are mostly within 5% (Figure S2 in the supporting information).



442 The cloud liquid and ice changes caused by dust INPs from each source are shown in Figure
443 11. Due to the strengthening of heterogeneous ice nucleation processes, INPs from all the three
444 sources consistently reduce the total liquid mass mixing ratio (TLIQ) (Figure 11, first column)
445 and cloud liquid droplet number concentration (NUMLIQ) (Figure 11, third column). The
446 influence of HLD is mainly in the lower troposphere (Fig. 11, top row) and the influence of LLD
447 extends to higher altitudes (Fig. 11, bottom two rows). Moreover, the cloud ice number
448 concentration (NUMICE) decreases in the upper troposphere (Figure 11, fourth column), likely
449 due to less cloud droplets available for the homogeneous freezing in cirrus cloud after
450 introducing dust INPs in the mixed-phase clouds. With fewer ice crystals falling from the cirrus
451 clouds to the mixed-phase clouds, the WBF process in the mixed-phase clouds is inhibited
452 (Figure S3). Other ice phase processes such as the accretion of cloud water by snow and the
453 growth of ice crystals by vapor deposition also become less efficient, which decreases the total
454 ice mass mixing ratio (TICE) above 600-700 hPa altitude (Figure 11, second column). TICE in
455 the lower troposphere is increased because of immersion freezing and snow sedimentation from
456 above.

457 Since liquid water path (LWP) is found to play a critical role in the Arctic radiative budget
458 (e.g., Dong et al., 2010; Hofer et al., 2019; Shupe and Intrieri, 2004), we further investigate the
459 seasonal variations of LWP changes caused by dust INPs from the three sources (Figure 12).
460 Corroborated with their large contribution to the immersion freezing rate during this time (Figure
461 10, top row), HLD INPs produce the strongest LWP decrease (-1.3 g m^{-2}) in boreal autumn
462 (Figure 12c), especially over North Canada and Greenland. The influence of LLD INPs on LWP
463 peaks in spring and winter. North African dust tends to have a larger impact on North Eurasia,
464 while East Asian dust impacts the west Arctic more.



465 Dust INPs from the three sources consistently increase (decrease) the annual mean
466 downwelling shortwave (longwave) radiative flux (FSDS and FLDS) at the surface (Figure 13,
467 left and middle columns). This is mainly due to the LWP decrease, which reduces the cloud
468 albedo and longwave cloud emissivity. For HLD INPs, the FLDS reduction dominates over the
469 FSDS increase and causes a net cooling effect at the Arctic surface (-0.24 W m^{-2}) (Figure 13c).
470 In contrast, FSDS and FLDS changes related to the LLD INPs are comparable, which cancels
471 each other and yields a small net radiative effect (0.08 W m^{-2} for NAF and -0.06 W m^{-2} for EAs)
472 (Figure 13, bottom two rows). These differences in the net radiative effect are associated with
473 different seasonalities of HLD and LLD. The insolation in the Arctic is strong in spring and
474 summer but very limited in autumn and winter. Since the HLD INPs have much stronger
475 influence on LWP in autumn and winter than spring and summer (Figure 12), their contribution
476 to the FSDS warming is weak and the FLDS cooling in autumn and winter dominates the annual
477 mean effect (Table 4, part 1; also seen in Figure S4 to S6). LLD INPs are also important in
478 spring and summer, so their FSDS warming effect is comparable to, and compensates for, the
479 FLDS cooling effect.

480 We also examined the dust INP effect on cloud radiative forcing (CRF) at the top of the
481 atmosphere (TOA) (Table 4, part 2). Dust INPs from the three sources induce a small net cooling
482 (from -0.03 to -0.05 W m^{-2}) in the Arctic, with SW warming and LW cooling effects. The net
483 cooling persists throughout the year, except for the summertime when the sufficient insolation
484 results in a strong SW warming and, consequently, a net warming effect. Shi and Liu (2019) also
485 found LLD can induce a generally net cooling effect above 70°N (0.18 to -1.95 W m^{-2}), but in a
486 much higher magnitude than the sum of NAF and EAs dust INP effects (-0.15 W m^{-2} above 70°N ,



487 not shown in Table 4), which implies the aerosol glaciation effect on mixed-phase clouds is
488 highly non-linear.

489 **4. Discussion**

490 The HLD emission in our CTRL simulation is manually tuned up by 10 times to match the
491 estimate by Bullard et al. (2016), which is derived by compiling field measurements in Iceland
492 and Alaska. Since the instruments were operated under extreme Arctic conditions and the
493 sampling is very scarce, this estimate may have large uncertainties. Therefore, the tuned HLD
494 emission can be biased as well. Considering the overestimation of Greenland dust deposition,
495 summertime surface dust concentrations at Alert station, and surface INP concentrations at
496 Svalbard, our tuning may cause a regional and temporal high bias in HLD dust emissions. We
497 examine this uncertainty by conducting a sensitivity experiment with halving HLD emissions in
498 CTRL (i.e., HLD_half) and analysing the interannual variability of CTRL and HLD_half
499 simulations (Table S2 and Figure S7-S8). The HLD_half simulation indeed has a better
500 performance than CTRL. However, the high bias for Greenland deposition and the summertime
501 overestimation of Alert dust surface concentration still exist, which reflects the limitation of the
502 dust emission parameterization we use. This parameterization may not be able to capture the
503 spatial distribution of dust emissions across the Arctic, considering that the model performance
504 at other sites (e.g., Heimaey, Figure 3a) is much better. Also, the HLD emissions and their
505 regional distributions have large interannual variabilities. Therefore, comparing model
506 simulations with measurements conducted in different years may result in large uncertainties.

507 The overestimation of surface dust and INP concentrations may imply a too weak vertical
508 transport of HLD, considering the low biases of dust in the upper troposphere as compared with



509 ARCTAS measurements and CALIPSO retrievals. The weak vertical transport at the source
510 regions in EAMv1 was also found in Wu et al. (2020), which was related to the too strong dry
511 deposition at the surface layer. If this bias is addressed, HLD would contribute less (more) to the
512 Arctic dust concentrations in the lower (upper) troposphere, which suggests a larger contribution
513 of HLD to the heterogeneous ice nucleation in the mixed-phase clouds in the summertime. As a
514 result, the HLD would induce a more positive net downwelling radiative flux at the surface in
515 summer and a less negative annual mean radiative effect. It is also noted that the underprediction
516 in the upper troposphere dust may come from a weak long-range transport of LLD. If this is the
517 case, the HLD would have a weaker contribution to the upper level dust concentrations and
518 likely less of an impact on mixed-phase cloud heterogeneous ice nucleation in the summertime.

519 In addition, EAMv1 has intrinsic biases in its cloud microphysics parameterizations. As
520 mentioned in Section 2.1, the WBF process rate in EAMv1 is tuned down by a factor of 10,
521 which results in too many supercooled liquid clouds in high latitudes (Y. Zhang et al., 2019; M.
522 Zhang et al., 2020). Shi and Liu (2019) found the sign and magnitude of dust INP cloud radiative
523 effect in the Arctic would change, after removing the tuning factor for the WBF process in
524 EAMv1. Moreover, EAMv1 does not account for several secondary ice production mechanisms,
525 which are suggested to have a large impact on the ice crystal number concentrations and thus
526 cloud phase (Zhao and Liu, 2021; Zhao et al., 2021b). All these uncertainties in the cloud
527 microphysical processes would influence our estimate of INP radiative effect and should be
528 addressed in future studies.



529 5. Conclusions

530 In this study, we investigate the source attribution of dust aerosols in the Arctic and quantify
531 the relative importance of Arctic local dust versus long-range transported LLD to the Arctic dust
532 loading and INP population. We found that HLD is responsible for 30.7% of the total dust
533 burden in the Arctic, whereas LLD from Asia and North Africa contributes 44.2% and 24.2%,
534 respectively. The vertical transport of HLD is limited due to the stable cold air in the Arctic and
535 thus it contributes more to the dust burden in the lower troposphere. In boreal summer and
536 autumn when the contribution of HLD is at a maximum because of stronger local dust emissions,
537 HLD is responsible for more than 30% of the Arctic dust loading below 800 hPa, but less than 10%
538 above 700 hPa. In contrast, LLD from North African and East Asian dust dominates the dust
539 burden in the free troposphere, since the poleward transport of LLD follows the uplifted
540 isentropes. The North African and East Asian dust accounts for about two thirds of the dust
541 loading above 700 hPa, with the remaining one third from other LLD sources. The North African
542 dust contributes more between 500 and 700 hPa, while the East Asian dust dominates in the
543 upper troposphere (above 400 hPa) because of its high emission heights. In addition, the North
544 Africa source has a larger contribution in springtime, while the other three seasons are more
545 influenced by the East Asian source.

546 Modeled dust INP concentrations are investigated following two ice nucleation
547 parameterizations: D15 and SM20. Compared with INP measurements, our results show that
548 including HLD as INPs significantly improves the model performance in simulating Arctic INP
549 concentrations, especially for the ground measurements and for the measurements conducted in
550 summer and autumn. We also examine the INP contributions from BC and SSA based on Sc20
551 and M18, respectively. The model suggests that both of them are only weak sources compared



552 with dust. We note that the model may underestimate SSA INPs and currently misses the
553 representation of terrestrial biological INPs. The model biases of INPs can also be due to bias in
554 simulating Arctic dust concentrations and/or the uncertainties in ice nucleation parameterizations.

555 We examine the contribution of dust from the three sources (Arctic, North Africa, and East
556 Asia) to the ambient immersion freezing rate in the Arctic. The contribution from HLD shows a
557 strong seasonal variation, with the peak contribution in boreal autumn (above 20% below 500
558 hPa). In summer, although HLD has strong contributions to the dust loading and INP
559 concentrations in the lower troposphere, its impact on the ambient immersion freezing rate is
560 limited due to the warm temperatures and weak vertical transport. This finding implies that
561 surface INP measurements may not be sufficient in representing the INP population in the Arctic
562 mixed-phase clouds and more measurements of INP vertical profiles are needed in the future.
563 North African and East Asian dust are the two major LLD contributors to the ambient immersion
564 freezing rate. The annual mean contribution (30-40%) from North African dust peaks at around
565 500 hPa, while the immersion freezing is dominated by East Asian dust (more than 40%) in the
566 upper troposphere (above 400 hPa).

567 The cloud glaciation effect of dust INPs from local Arctic sources, and North African and East
568 Asian sources, is further examined. It is found that INPs from all the three sources consistently
569 result in a reduction in TLIQ and NUMLIQ. TICE and NUMICE at higher altitude also decrease,
570 likely due to the weakening of homogeneous freezing in cirrus clouds. LWP reduction caused by
571 HLD INPs is evident in autumn and winter, while those by dust INPs from the two LLD sources
572 peak in spring. HLD INPs also drive a net cooling effect of -0.24 W m^{-2} in the downwelling
573 radiative flux at the surface in the Arctic, while the net radiative effects of the two LLD INP
574 sources are relatively small (0.08 W m^{-2} for NAF and -0.06 W m^{-2} for EAs). This variation in



575 radiative effect reflects the seasonal difference between HLD and LLD. Our results also suggest
576 that all the three dust sources result in a weak negative net cloud radiative effect (-0.03 to -0.05
577 W m^{-2}) in the Arctic, which is consistent with Shi and Liu (2019).

578 Overall, our study shows that the Arctic local dust, which has been overlooked in previous
579 studies, may have large contributions to the Arctic dust loading and INP population. It can also
580 influence the Arctic mixed-phase cloud properties by acting as INPs. Considering the climate
581 impacts of local Arctic dust emissions will be important given a warming climate, where
582 reduction in snow coverage and more exposure of dryland in the Arctic may lead to increased
583 HLD emissions.

584 *Code availability.* The E3SM code is available on GitHub: [https://github.com/E3SM-](https://github.com/E3SM-Project/E3SM.git)
585 [Project/E3SM.git](https://github.com/E3SM-Project/E3SM.git).

586 *Author contribution.* YS and XL conceived the project. YS modified the code, conducted the
587 simulations, and led the analyses with suggestions from XL, MW, ZK, and HB. XL supervised
588 the study. YS wrote the first draft of the paper. All coauthors were involved in helpful
589 discussions and revised the paper.

590 *Competing interests.* The authors declare that they have no conflict of interest.

591 *Acknowledgements.* The authors would like to thank Drs. Xi Zhao, Meng Zhang, and Sarah
592 Brooks for their comments and suggestions. Mingxuan Wu is supported by the US Department
593 of Energy (DOE), Office of Biological and Environmental Research, Earth and Environmental
594 System Modeling program as part of the Energy Exascale Earth System Model (E3SM) project.



595 The Pacific Northwest National Laboratory (PNNL) is operated for DOE by the Battelle
596 Memorial Institute under contract DE-AC05-76RLO1830. This research used resources of the
597 National Energy Research Scientific Computing Center, a DOE Office of Science User Facility
598 supported by the Office of Science of the U.S. Department of Energy under contract DE-AC02-
599 05CH11231.

600 *Financial support.* This research was supported by the DOE Atmospheric System Research
601 (ASR) Program (grants DE-SC0020510 and DE-SC0021211).

602 **References**

603 Albani, S., Mahowald, N. M., Perry, A. T., Scanza, R. A., Zender, C. S., Heavens, N. G., Maggi,
604 V., Kok, J. F., and Otto-Bliesner, B. L.: Improved dust representation in the Community
605 Atmosphere Model, *J. Adv. Model. Earth Syst.*, 6, 541–570,
606 <https://doi.org/10.1002/2013MS000279>, 2014.

607 Arimoto, R., Duce, R. A., Ray, B. J., Ellis Jr, W. G., Cullen, J. D., and Merrill, J. T.: Trace
608 elements in the atmosphere over the North Atlantic, *J. Geophys. Res. Atmos.*, 100(D1), 1199–
609 1213, <https://doi.org/10.1029/94JD02618>, 1995.

610 Arnalds, O., Dagsson-Waldhauserova, P., and Olafsson, H.: The Icelandic volcanic aeolian
611 environment: Processes and impacts — A review, *Aeolian Res.*, 20, 176–195,
612 <https://doi.org/10.1016/j.aeolia.2016.01.004>, 2016.

613 Atkinson, J. D., Murray, B. J., Woodhouse, M. T., Whale, T. F., Baustian, K. J., Carslaw, K. S.,
614 Dobbie, S., O’Sullivan, D., and Malkin, T. L.: The importance of feldspar for ice nucleation by
615 mineral dust in mixed-phase clouds, *Nature*, 498, 355–358, <https://doi.org/10.1038/nature12278>,
616 2013.

617 Baddock, M. C., Mockford, T., Bullard, J. E., and Thorsteinsson, T.: Pathways of high-latitude
618 dust in the North Atlantic, *Earth Planet. Sci. Lett.*, 459, 170–182,
619 <https://doi.org/10.1016/j.epsl.2016.11.034>, 2017.

620 de Boer, G., Morrison, H., Shupe, M. D., and Hildner, R.: Evidence of liquid dependent ice
621 nucleation in high-latitude stratiform clouds from surface remote sensors, *Geophys. Res. Lett.*,
622 38, L01803, <https://doi.org/10.1029/2010GL046016>, 2011.

623 Bogenschutz, P. A., Gettelman, A., Morrison, H., Larson, V. E., Craig, C., and Schanen, D. P.:
624 Higher-order turbulence closure and its impact on climate simulations in the community
625 atmosphere model, *J. Clim.*, 26, 9655–9676, <https://doi.org/10.1175/JCLI-D-13-00075.1>, 2013.



- 626 Bory, A. J.-M., Biscaye, P. E., Svensson, A., and Grousset, F. E.: Seasonal variability in the
627 origin of recent atmospheric mineral dust at NorthGRIP, Greenland, *Earth Planet. Sci. Lett.*, 196,
628 123–134, [https://doi.org/10.1016/S0012-821X\(01\)00609-4](https://doi.org/10.1016/S0012-821X(01)00609-4), 2002.
- 629 Bory, A. J.-M., Biscaye, P. E., and Grousset, F. E.: Two distinct seasonal Asian source regions
630 for mineral dust deposited in Greenland (NorthGRIP), *Geophys. Res. Lett.*, 30,
631 <https://doi.org/10.1029/2002GL016446>, 2003.
- 632 Breider, T. J., Mickley, L. J., Jacob, D. J., Wang, Q., Fisher, J. A., Chang, R. Y.-W., and
633 Alexander, B.: Annual distributions and sources of Arctic aerosol components, aerosol optical
634 depth, and aerosol absorption, *J. Geophys. Res. Atmos.*, 119, 4107–4124,
635 <https://doi.org/10.1002/2013JD020996>, 2014.
- 636 Bullard, J. E.: The distribution and biogeochemical importance of high-latitude dust in the Arctic
637 and Southern Ocean-Antarctic regions, *J. Geophys. Res. Atmos.*, 122, 3098–3103,
638 <https://doi.org/10.1002/2016JD026363>, 2017.
- 639 Bullard, J. E. and Austin, M. J.: Dust generation on a proglacial floodplain, West Greenland,
640 *Aeolian Res.*, 3, 43–54, <https://doi.org/10.1016/j.aeolia.2011.01.002>, 2011.
- 641 Bullard, J. E., Baddock, M., Bradwell, T., Crusius, J., Darlington, E., Gaiero, D., Gassó, S.,
642 Gísladóttir, G., Hodgkins, R., McCulloch, R., McKenna-Neuman, C., Mockford, T., Stewart, H.,
643 and Thorsteinsson, T.: High-latitude dust in the Earth system, *Rev. Geophys.*, 54, 447–485,
644 <https://doi.org/10.1002/2016RG000518>, 2016.
- 645 Creamean, J. M., Kirpes, R. M., Pratt, K. A., Spada, N. J., Maahn, M., de Boer, G., Schnell, R.
646 C., and China, S.: Marine and terrestrial influences on ice nucleating particles during continuous
647 springtime measurements in an Arctic oilfield location, *Atmos. Chem. Phys.*, 18, 18023–18042,
648 <https://doi.org/10.5194/acp-18-18023-2018>, 2018.
- 649 Creamean, J. M., Hill, T. C. J., DeMott, P. J., Uetake, J., Kreidenweis, S., and Douglas, T. A.:
650 Thawing permafrost: an overlooked source of seeds for Arctic cloud formation, *Environ. Res.
651 Lett.*, 15, 084022, <https://doi.org/10.1088/1748-9326/ab87d3>, 2020.
- 652 Crusius, J., Schroth, A. W., Gassó, S., Moy, C. M., Levy, R. C., and Gatica, M.: Glacial flour
653 dust storms in the Gulf of Alaska: Hydrologic and meteorological controls and their importance
654 as a source of bioavailable iron, *Geophys. Res. Lett.*, 38, L06602,
655 <https://doi.org/10.1029/2010GL046573>, 2011.
- 656 Dagsson-Waldhauserova, P., Arnalds, O., and Olafsson, H.: Long-term variability of dust events
657 in Iceland (1949–2011), *Atmos. Chem. Phys.*, 14, 13411–13422, <https://doi.org/10.5194/acp-14-13411-2014>, 2014.
- 659 DeMott, P. J., Sassen, K., Poellot, M. R., Baumgardner, D., Rogers, D. C., Brooks, S. D., Prenni,
660 A. J., and Kreidenweis, S. M.: African dust aerosols as atmospheric ice nuclei, *Geophys. Res.
661 Lett.*, 30(14), 1732, <https://doi.org/10.1029/2003GL017410>, 2003.



- 662 DeMott, P. J., Prenni, A. J., Liu, X., Kreidenweis, S. M., Petters, M. D., Twohy, C. H.,
663 Richardson, M. S., Eidhammer, T., and Rogers, D. C.: Predicting global atmospheric ice nuclei
664 distributions and their impacts on climate, *Proc. Natl. Acad. Sci. U.S.A.*, 107(25), 11217–11222,
665 <https://doi.org/10.1073/pnas.0910818107>, 2010.
- 666 DeMott, P. J., Prenni, A. J., McMeeking, G. R., Sullivan, R. C., Petters, M. D., Tobo, Y.,
667 Niemand, M., Möhler, O., Snider, J. R., Wang, Z., and Kreidenweis, S. M.: Integrating
668 laboratory and field data to quantify the immersion freezing ice nucleation activity of mineral
669 dust particles, *Atmos. Chem. Phys.*, 15, 393–409, <https://doi.org/10.5194/acp-15-393-2015>, 2015.
- 670 Dong, X., Xi, B., Crosby, K., Long, C. N., Stone, R. S., and Shupe, M. D.: A 10 year
671 climatology of Arctic cloud fraction and radiative forcing at Barrow, Alaska, *J. Geophys. Res.*
672 *Atmos.*, 115, D17212, <https://doi.org/10.1029/2009JD013489>, 2010.
- 673 Dörnbrack, A., Stachlewska, I. S., Ritter, C., and Neuber, R.: Aerosol distribution around
674 Svalbard during intense easterly winds, *Atmos. Chem. Phys.*, 10, 1473–1490,
675 <https://doi.org/10.5194/acp-10-1473-2010>, 2010.
- 676 Fan, S.-M.: Modeling of observed mineral dust aerosols in the arctic and the impact on winter
677 season low-level clouds, *J. Geophys. Res. Atmos.*, 118, 11161–11174,
678 <https://doi.org/10.1002/jgrd.50842>, 2013.
- 679 Fenn, R. W. and Weickmann, H. K.: Some results of aerosol measurements, *Geofisica Pura e*
680 *Applicata*, 42, 53–61, <https://doi.org/10.1007/BF02113389>, 1959.
- 681 Gettelman, A. and Morrison, H.: Advanced two-moment bulk microphysics for global models.
682 Part I: off-line tests and comparison with other schemes, *J. Clim.*, 28, 1268–1287,
683 <https://doi.org/10.1175/JCLI-D-14-00102.1>, 2015.
- 684 Ghan, S. J. and Zaveri, R. A.: Parameterization of optical properties for hydrated internally
685 mixed aerosol, *J. Geophys. Res.*, 112, D10201, <https://doi.org/10.1029/2006JD007927>, 2007.
- 686 Ginoux, P., Chin, M., Tegen, I., Prospero, J. M., Holben, B., Dubovik, O., and Lin, S.-J.: Sources
687 and distributions of dust aerosols simulated with the GOCART model, *J. Geophys. Res.*, 106,
688 20255–20273, <https://doi.org/10.1029/2000JD000053>, 2001.
- 689 Golaz, J.-C., Larson, V. E., and Cotton, W. R.: A PDF-based model for boundary layer clouds.
690 Part I: Method and model description, *J. Atmos. Sci.*, 59, 3540–3551,
691 [https://doi.org/10.1175/1520-0469\(2002\)059<3540:APBMFB>2.0.CO;2](https://doi.org/10.1175/1520-0469(2002)059<3540:APBMFB>2.0.CO;2), 2002.
- 692 Groot Zwaafink, C. D., Grythe, H., Skov, H., and Stohl, A.: Substantial contribution of northern
693 high-latitude sources to mineral dust in the Arctic, *J. Geophys. Res. Atmos.*, 121, 13678–13697,
694 <https://doi.org/10.1002/2016JD025482>, 2016.
- 695 Hiranuma, N., Brooks, S. D., Moffet, R. C., Glen, A., Laskin, A., Gilles, M. K. m Liu, P.,
696 Macdonald, A. M., Strapp, J. W., McFarquhar, G. M: Chemical characterization of individual
697 particles and residuals of cloud droplets and ice crystals collected on board research aircraft in



- 698 the ISDAC 2008 study, *J. Geophys. Res. Atmos.*, 118, 6564–6579,
699 <https://doi.org/10.1002/jgrd.50484>, 2013.
- 700 Hofer, S., Tedstone, A. J., Fettweis, X., and Bamber, J. L.: Cloud microphysics and circulation
701 anomalies control differences in future Greenland melt, *Nat. Clim. Chang.*, 9, 523–528,
702 <https://doi.org/10.1038/s41558-019-0507-8>, 2019.
- 703 Holben, B. N., Eck, T. F., Slutsker, I., Tanré, D., Buis, J. P., Setzer, A., Vermote, E., Reagan, J.
704 A., Kaufman, Y. J., Nakajima, T., Lavenu, F., Jankowiak, I., and Smirnov, A.: AERONET—A
705 Federated Instrument Network and Data Archive for Aerosol Characterization, *Remote Sens.*
706 *Environ.*, 66, 1–16, [https://doi.org/10.1016/S0034-4257\(98\)00031-5](https://doi.org/10.1016/S0034-4257(98)00031-5), 1998.
- 707 Hoose, C. and Möhler, O.: Heterogeneous ice nucleation on atmospheric aerosols: a review of
708 results from laboratory experiments, *Atmos. Chem. Phys.*, 12, 9817–9854,
709 <https://doi.org/10.5194/acp-12-9817-2012>, 2012.
- 710 Huang, Z., Huang, J., Hayasaka, T., Wang, S., Zhou, T., and Jin, H.: Short-cut transport path for
711 Asian dust directly to the Arctic: a case study, *Environ. Res. Lett.*, 10, 114018,
712 <https://doi.org/10.1088/1748-9326/10/11/114018>, 2015.
- 713 Huneus, N., Schulz, M., Balkanski, Y., Griesfeller, J., Prospero, J., Kinne, S., Bauer, S.,
714 Boucher, O., Chin, M., Dentener, F., Diehl, T., Easter, R., Fillmore, D., Ghan, S., Ginoux, P.,
715 Grini, A., Horowitz, L., Koch, D., Krol, M. C., Landing, W., Liu, X., Mahowald, N., Miller, R.,
716 Morcrette, J.-J., Myhre, G., Penner, J., Perlwitz, J., Stier, P., Takemura, T., and Zender, C. S.:
717 Global dust model intercomparison in AeroCom phase I, *Atmos. Chem. Phys.*, 11, 7781–7816,
718 <https://doi.org/10.5194/acp-11-7781-2011>, 2011.
- 719 Irish, V. E., Hanna, S. J., Willis, M. D., China, S., Thomas, J. L., Wentzell, J. J. B., Cirisan, A.,
720 Si, M., Leaitch, W. R., Murphy, J. G., Abbatt, J. P. D., Laskin, A., Girard, E., and Bertram, A. K.:
721 Ice nucleating particles in the marine boundary layer in the Canadian Arctic during summer 2014,
722 *Atmos. Chem. Phys.*, 19, 1027–1039, <https://doi.org/10.5194/acp-19-1027-2019>, 2019.
- 723 Jacob, D. J., Crawford, J. H., Maring, H., Clarke, A. D., Dibb, J. E., Emmons, L. K., Ferrare, R.
724 A., Hostetler, C. A., Russell, P. B., Singh, H. B., Thompson, A. M., Shaw, G. E., McCauley, E.,
725 Pederson, J. R., and Fisher, J. A.: The Arctic Research of the Composition of the Troposphere
726 from Aircraft and Satellites (ARCTAS) mission: design, execution, and first results, *Atmos.*
727 *Chem. Phys.*, 10, 5191–5212, <https://doi.org/10.5194/acp-10-5191-2010>, 2010.
- 728 Kinne, S., Schulz, M., Textor, C., Guibert, S., Balkanski, Y., Bauer, S. E., Berntsen, T., Berglen,
729 T. F., Boucher, O., Chin, M., Collins, W., Dentener, F., Diehl, T., Easter, R., Feichter, J.,
730 Fillmore, D., Ghan, S., Ginoux, P., Gong, S., Grini, A., Hendricks, J., Herzog, M., Horowitz, L.,
731 Isaksen, I., Iversen, T., Kirkevåg, A., Kloster, S., Koch, D., Kristjansson, J. E., Krol, M., Lauer,
732 A., Lamarque, J. F., Lesins, G., Liu, X., Lohmann, U., Montanaro, V., Myhre, G., Penner, J.,
733 Pitari, G., Reddy, S., Seland, O., Stier, P., Takemura, T., and Tie, X.: An AeroCom initial
734 assessment – optical properties in aerosol component modules of global models, *Atmos. Chem.*
735 *Phys.*, 6, 1815–1834, <https://doi.org/10.5194/acp-6-1815-2006>, 2006.



- 736 Kohfeld, K. E. and Harrison, S. P.: DIRTMAP: the geological record of dust, *Earth-Sci. Rev.*, 54,
737 81–114, [https://doi.org/10.1016/S0012-8252\(01\)00042-3](https://doi.org/10.1016/S0012-8252(01)00042-3), 2001.
- 738 Kok, J. F.: A scaling theory for the size distribution of emitted dust aerosols suggests climate
739 models underestimate the size of the global dust cycle, *Proc. Natl. Acad. Sci. U.S.A.*, 108(3),
740 1016–1021, <https://doi.org/10.1073/pnas.1014798108>, 2011.
- 741 Kok, J. F., Mahowald, N. M., Fratini, G., Gillies, J. A., Ishizuka, M., Leys, J. F., Mikami, M.,
742 Park, M.-S., Park, S.-U., Van Pelt, R. S., and Zobeck, T. M.: An improved dust emission model –
743 Part 1: Model description and comparison against measurements, *Atmos. Chem. Phys.*, 14,
744 13023–13041, <https://doi.org/10.5194/acp-14-13023-2014>, 2014a.
- 745 Kok, J. F., Albani, S., Mahowald, N. M., and Ward, D. S.: An improved dust emission model –
746 Part 2: Evaluation in the Community Earth System Model, with implications for the use of dust
747 source functions, *Atmos. Chem. Phys.*, 14, 13043–13061, <https://doi.org/10.5194/acp-14-13043-2014>, 2014b.
- 749 Kok, J. F., Ridley, D. A., Zhou, Q., Miller, R. L., Zhao, C., Heald, C. L., Ward, D. S., Albani, S.,
750 and Haustein, K.: Smaller desert dust cooling effect estimated from analysis of dust size and
751 abundance, *Nat. Geosci.*, 10, 274–278, <https://doi.org/10.1038/ngeo2912>, 2017.
- 752 Larson, V. E., Golaz, J.-C., and Cotton, W. R.: Small-Scale and Mesoscale Variability in Cloudy
753 Boundary Layers: Joint Probability Density Functions, *J. Atmos. Sci.*, 59, 3519–3539,
754 [https://doi.org/10.1175/1520-0469\(2002\)059<3519:SSAMVI>2.0.CO;2](https://doi.org/10.1175/1520-0469(2002)059<3519:SSAMVI>2.0.CO;2), 2002.
- 755 Liu, X., Xie, S., Boyle, J., Klein, S. A., Shi, X., Wang, Z., Lin, W., Ghan, S. J., Earle, M., Liu, P.
756 S. K., and Zelenyuk, A.: Testing cloud microphysics parameterizations in NCAR CAM5 with
757 ISDAC and M-PACE observations, *J. Geophys. Res.*, 116, D00T11,
758 <https://doi.org/10.1029/2011JD015889>, 2011.
- 759 Liu, X., Ma, P.-L., Wang, H., Tilmes, S., Singh, B., Easter, R. C., Ghan, S. J., and Rasch, P. J.:
760 Description and evaluation of a new four-mode version of the Modal Aerosol Module (MAM4)
761 within version 5.3 of the Community Atmosphere Model, *Geosci. Model Dev.*, 9, 505–522,
762 <https://doi.org/10.5194/gmd-9-505-2016>, 2016.
- 763 Luo, C., Mahowald, N. M., and Corral, J. del: Sensitivity study of meteorological parameters on
764 mineral aerosol mobilization, transport, and distribution, *J. Geophys. Res.*, 108, 4447,
765 <https://doi.org/10.1029/2003JD003483>, 2003.
- 766 Luo, T., Wang, Z., Ferrare, R. A., Hostetler, C. A., Yuan, R., and Zhang, D.: Vertically resolved
767 separation of dust and other aerosol types by a new lidar depolarization method, *Opt. Express*, 23,
768 14095–14107, <https://doi.org/10.1364/OE.23.014095>, 2015a.
- 769 Luo, T., Wang, Z., Zhang, D., Liu, X., Wang, Y., and Yuan, R.: Global dust distribution from
770 improved thin dust layer detection using A-train satellite lidar observations, *Geophys. Res. Lett.*,
771 42, 620–628, <https://doi.org/10.1002/2014GL062111>, 2015b.



- 772 Maenhaut, W., Fernandez-Jimenez, M.-T., Rajta, I., Dubtsov, S., Meixner, F. X., Andreae, M. O.,
773 Torr, S., Hargrove, J. W., Chimanga, P., and Mlambo, J.: Long-term aerosol composi- tion
774 measruments and source apportionment at Rukomechi, Zim- babwe, J. Aerosol Sci., 31(Suppl. 1),
775 S469–S470, 2000a.
- 776 Maenhaut, W., Fernandez-Jimenez, M.-T., Vanderzalm, J. L., Hooper, B. M., Hooper, M. A.,
777 and Tapper, N. J.: Aerosol com- position at Jabiru, Australia and impact of biomass burning, J.
778 Aerosol Sci., 31(Suppl. 1), S745–S746, 2000b.
- 779 Mahowald, N. M., Engelstaedter, S., Luo, C., Sealy, A., Artaxo, P., Benitez-Nelson, C., Bonnet,
780 S., Chen, Y., Chuang, P. Y., Cohen, D. D., Dulac, F., Herut, B., Johansen, A. M., Kubilay, N.,
781 Losno, R., Maenhaut, W., Paytan, A., Prospero, J. M., Shank, L. M., and Siefert, R. L.:
782 Atmospheric iron deposition: global distribution, variability, and human perturbations, *Ann. Rev.*
783 *Mar. Sci.*, 1, 245–278, <https://doi.org/10.1146/annurev.marine.010908.163727>, 2009.
- 784 Mason, R. H., Si, M., Chou, C., Irish, V. E., Dickie, R., Elizondo, P., Wong, R., Brintnell, M.,
785 Elsasser, M., Lassar, W. M., Pierce, K. M., Leaitch, W. R., MacDonald, A. M., Platt, A., Toom-
786 Sauntry, D., Sarda-Estève, R., Schiller, C. L., Suski, K. J., Hill, T. C. J., Abbatt, J. P. D.,
787 Huffman, J. A., DeMott, P. J., and Bertram, A. K.: Size-resolved measurements of ice-nucleating
788 particles at six locations in North America and one in Europe, *Atmos. Chem. Phys.*, 16, 1637–
789 1651, <https://doi.org/10.5194/acp-16-1637-2016>, 2016.
- 790 McCluskey, C. S., Ovadnevaite, J., Rinaldi, M., Atkinson, J., Belosi, F., Ceburnis, D., Marullo,
791 S., Hill, T. C. J., Lohmann, U., Kanji, Z. A., O’Dowd, C., Kreidenweis, S. M., and DeMott, P. J.:
792 Marine and terrestrial organic ice-nucleating particles in pristine marine to continentally
793 influenced Northeast Atlantic air masses, *J. Geophys. Res. Atmos.*, 123, 6196–6212,
794 <https://doi.org/10.1029/2017JD028033>, 2018.
- 795 McFarquhar, G. M., Ghan, S., Verlinde, J., Korolev, A., Strapp, J. W., Schmid, B., Tomlinson, J.
796 M., Wolde, M., Brooks, S. D., Cziczo, D., Dubey, M. K., Fan, J., Flynn, C., Gultepe, I., Hubbe,
797 J., Gilles, M. K., Laskin, A., Lawson, P., Leaitch, W. R., Liu, P., Liu, X., Lubin, D., Mazzoleni,
798 C., Macdonald, A.-M., Moffet, R. C., Morrison, H., Ovchinnikov, M., Shupe, M. D., Turner, D.
799 D., Xie, S., Zelenyuk, A., Bae, K., Freer, M., and Glen, A.: Indirect and Semi-direct Aerosol
800 Campaign: The Impact of Arctic Aerosols on Clouds, *Bull. Amer. Meteor. Soc.*, 92, 183–201,
801 <https://doi.org/10.1175/2010BAMS2935.1>, 2011.
- 802 Morrison, H., de Boer, G., Feingold, G., Harrington, J., Shupe, M. D., and Sulia, K.: Resilience
803 of persistent Arctic mixed-phase clouds, *Nat. Geosci.*, 5, 11–17,
804 <https://doi.org/10.1038/ngeo1332>, 2012.
- 805 Murray, B. J., O’Sullivan, D., Atkinson, J. D., and Webb, M. E.: Ice nucleation by particles
806 immersed in supercooled cloud droplets, *Chem. Soc. Rev.*, 41, 6519–6554,
807 <https://doi.org/10.1039/c2cs35200a>, 2012.
- 808 Paramonov, M., David, R. O., Kretzschmar, R., and Kanji, Z. A.: A laboratory investigation of
809 the ice nucleation efficiency of three types of mineral and soil dust, *Atmos. Chem. Phys.*, 18,
810 16515–16536, <https://doi.org/10.5194/acp-18-16515-2018>, 2018.



- 811 Prenni, A. J., Harrington, J. Y., Tjernström, M., DeMott, P. J., Avramov, A., Long, C. N.,
812 Kreidenweis, S. M., Olsson, P. Q., and Verlinde, J.: Can ice-nucleating aerosols affect Arctic
813 seasonal climate?, *Bull. Amer. Meteor. Soc.*, 88, 541–550, [https://doi.org/10.1175/BAMS-88-4-](https://doi.org/10.1175/BAMS-88-4-541)
814 541, 2007.
- 815 Prenni, A. J., Demott, P. J., Rogers, D. C., Kreidenweis, S. M., Mcfarquhar, G. M., Zhang, G.,
816 and Poellot, M. R.: Ice nuclei characteristics from M-PACE and their relation to ice formation in
817 clouds, *Tellus B*, 61, 436–448, <https://doi.org/10.1111/j.1600-0889.2009.00415.x>, 2009.
- 818 Prospero, J. M.: The Atmospheric Transport of Particles to the Ocean, in: *Particle Flux in the*
819 *Ocean*, edited by: Ittekkot, V., Schäfer, P., Honjo, S., and Depetris, P. J., John Wiley & Sons
820 Ltd., New York, 1996.
- 821 Prospero, J. M., Bullard, J. E., and Hodgkins, R.: High-Latitude Dust Over the North Atlantic:
822 Inputs from Icelandic Proglacial Dust Storms, *Science*, 335, 1078–1082,
823 <https://doi.org/10.1126/science.1217447>, 2012.
- 824 Prospero, J. M., Uematsu, M., and Savoie, D. L.: Mineral aerosol transport to the Pacific Ocean,
825 edited by: Riley, J. P., 187–218, Academic Press, New York, 1989.
- 826 Rasch, P. J., Xie, S., Ma, P. -L., Lin, W., Wang, H., Tang, Q., Burrows, S. M., Caldwell, P.,
827 Zhang, K., Easter, R. C., Cameron-Smith, P., Singh, B., Wan, H., Golaz, J. -C., Harrop, B. E.,
828 Roesler, E., Bacmeister, J., Larson, V. E., Evans, K. J., Qian, Y., Taylor, M., Leung, L. R.,
829 Zhang, Y., Brent, L., Branstetter, M., Hannay, C., Mahajan, S., Mametjanov, A., Neale, R.,
830 Richter, J. H., Yoon, J. -H., Zender, C. S., Bader, D., Flanner, M., Foucar, J. G., Jacob, R., Keen,
831 N., Klein, S. A., Liu, X., Salinger, A. G., Shrivastava, M., and Yang, Y.: An overview of the
832 atmospheric component of the Energy Exascale Earth System Model, *J. Adv. Model. Earth Syst.*,
833 11, 2377–2411, <https://doi.org/10.1029/2019MS001629>, 2019.
- 834 Ridley, D. A., Heald, C. L., Kok, J. F., and Zhao, C.: An observationally constrained estimate of
835 global dust aerosol optical depth, *Atmos. Chem. Phys.*, 16, 15097–15117,
836 <https://doi.org/10.5194/acp-16-15097-2016>, 2016.
- 837 Sanchez-Marroquin, A., Arnalds, O., Baustian-Dorsi, K. J., Browse, J., Dagsson-Waldhauserova,
838 P., Harrison, A. D., Maters, E. C., Pringle, K. J., Vergara-Temprado, J., Burke, I. T., McQuaid, J.
839 B., Carslaw, K. S., and Murray, B. J.: Iceland is an episodic source of atmospheric ice-nucleating
840 particles relevant for mixed-phase clouds, *Sci. Adv.*, 6, eaba8137,
841 <https://doi.org/10.1126/sciadv.aba8137>, 2020.
- 842 Schill, G. P., DeMott, P. J., Emerson, E. W., Rauker, A. M. C., Kodros, J. K., Suski, K. J., Hill, T.
843 C. J., Levin, E. J. T., Pierce, J. R., Farmer, D. K., and Kreidenweis, S. M.: The contribution of
844 black carbon to global ice nucleating particle concentrations relevant to mixed-phase clouds,
845 *Proc. Natl. Acad. Sci. U.S.A.*, 117, 22705–22711, <https://doi.org/10.1073/pnas.2001674117>,
846 2020.



- 847 Shao, Y., Wyrwoll, K.-H., Chappell, A., Huang, J., Lin, Z., McTainsh, G. H., Mikami, M.,
848 Tanaka, T. Y., Wang, X., and Yoon, S.: Dust cycle: An emerging core theme in Earth system
849 science, *Aeolian Res.*, 2, 181–204, <https://doi.org/10.1016/j.aeolia.2011.02.001>, 2011.
- 850 Shi, Y. and Liu, X.: Dust Radiative Effects on Climate by Glaciating Mixed-Phase Clouds,
851 *Geophys. Res. Lett.*, 46, 6128–6137, <https://doi.org/10.1029/2019GL082504>, 2019.
- 852 Shupe, M. D. and Intrieri, J. M.: Cloud Radiative Forcing of the Arctic Surface: The Influence of
853 Cloud Properties, Surface Albedo, and Solar Zenith Angle, *J. Clim.*, 17, 616–628,
854 [https://doi.org/10.1175/1520-0442\(2004\)017<0616:CRFOTA>2.0.CO;2](https://doi.org/10.1175/1520-0442(2004)017<0616:CRFOTA>2.0.CO;2), 2004.
- 855 Si, M., Evoy, E., Yun, J., Xi, Y., Hanna, S. J., Chivulescu, A., Rawlings, K., Veber, D., Platt, A.,
856 Kunkel, D., Hoor, P., Sharma, S., Leaitch, W. R., and Bertram, A. K.: Concentrations,
857 composition, and sources of ice-nucleating particles in the Canadian High Arctic during spring
858 2016, *Atmos. Chem. Phys.*, 19, 3007–3024, <https://doi.org/10.5194/acp-19-3007-2019>, 2019.
- 859 Stohl, A.: Characteristics of atmospheric transport into the Arctic troposphere, *J. Geophys. Res.*,
860 111, D11306, <https://doi.org/10.1029/2005JD006888>, 2006.
- 861 Stone, R., Anderson, G., Andrews, E., Dutton, E., Harris, J., Shettle, E., Berk, A.: Asian dust
862 signatures at Barrow: observed and simulated. Incursions and impact of Asian dust over
863 Northern Alaska, Workshop on Remote Sensing of Atmospheric Aerosols, IEEE Workshop on
864 Remote Sensing of Atmospheric Aerosols, 74-79,
865 <https://doi.org/10.1109/AERSOL.2005.1494152>, 2005.
- 866 Tan, I. and Storelvmo, T.: Evidence of Strong Contributions from Mixed-Phase Clouds to Arctic
867 Climate Change, *Geophys. Res. Lett.*, 46, 2894–2902, <https://doi.org/10.1029/2018GL081871>,
868 2019.
- 869 Tanaka, T. Y. and Chiba, M.: A numerical study of the contributions of dust source regions to
870 the global dust budget, *Glob. Planet. Change*, 52, 88–104,
871 <https://doi.org/10.1016/j.gloplacha.2006.02.002>, 2006.
- 872 Tegen, I., Harrison, S. P., Kohfeld, K., Prentice, I. C., Coe, M., and Heimann, M.: Impact of
873 vegetation and preferential source areas on global dust aerosol: Results from a model study, *J.*
874 *Geophys. Res. Atmos.*, 107, AAC 14-1-AAC 14-27, <https://doi.org/10.1029/2001JD000963>,
875 2002.
- 876 Tobo, Y., Adachi, K., DeMott, P. J., Hill, T. C. J., Hamilton, D. S., Mahowald, N. M., Nagatsuka,
877 N., Ohata, S., Uetake, J., Kondo, Y., and Koike, M.: Glacially sourced dust as a potentially
878 significant source of ice nucleating particles, *Nat. Geosci.*, 12, 253–258,
879 <https://doi.org/10.1038/s41561-019-0314-x>, 2019.
- 880 Vali, G.: Nucleation terminology, *Bull. Am. Meteorol. Soc.*, 66, 1426–1427, 1985.
- 881 Vali, G., DeMott, P. J., Möhler, O., and Whale, T. F.: Technical Note: A proposal for ice
882 nucleation terminology, *Atmos. Chem. Phys.*, 15, 10263–10270, [https://doi.org/10.5194/acp-15-](https://doi.org/10.5194/acp-15-10263-2015)
883 10263-2015, 2015.



- 884 VanCuren, R. A., Cahill, T., Burkhart, J., Barnes, D., Zhao, Y., Perry, K., Cliff, S., and
885 McConnell, J.: Aerosols and their sources at Summit Greenland – First results of continuous
886 size- and time-resolved sampling, *Atmos. Environ.*, 52, 82–97,
887 <https://doi.org/10.1016/j.atmosenv.2011.10.047>, 2012.
- 888 Wang, H., Rasch, P. J., Easter, R. C., Singh, B., Zhang, R., Ma, P.-L., Qian, Y., Ghan, S. J., and
889 Beagley, N.: Using an explicit emission tagging method in global modeling of source-receptor
890 relationships for black carbon in the Arctic: Variations, sources, and transport pathways, *J.*
891 *Geophys. Res. Atmos.*, 119, 12888–12909, <https://doi.org/10.1002/2014JD022297>, 2014.
- 892 Wang, H., Easter, R. C., Zhang, R., Ma, P.-L., Singh, B., Zhang, K., Ganguly, D., Rasch, P. J.,
893 Burrows, S. M., Ghan, S. J., Lou, S., Qian, Y., Yang, Y., Feng, Y., Flanner, M., Leung, L. R.,
894 Liu, X., Shrivastava, M., Sun, J., Tang, Q., Xie, S., and Yoon, J.: Aerosols in the E3SM Version
895 1: New Developments and Their Impacts on Radiative Forcing, *J. Adv. Model. Earth Syst.*, 12,
896 e2019MS001851, <https://doi.org/10.1029/2019MS001851>, 2020.
- 897 Wang, Y., Liu, X., Hoose, C., and Wang, B.: Different contact angle distributions for
898 heterogeneous ice nucleation in the Community Atmospheric Model version 5, *Atmos. Chem.*
899 *Phys.*, 14, 10411–10430, <https://doi.org/10.5194/acp-14-10411-2014>, 2014.
- 900 Westbrook, C. D. and Illingworth, A. J.: The formation of ice in a long-lived supercooled layer
901 cloud: Ice Formation in Altocumulus, *Q. J. R. Meteorol. Soc.*, 139, 2209–2221,
902 <https://doi.org/10.1002/qj.2096>, 2013.
- 903 Wilson, T. W., Ladino, L. A., Alpert, P. A., Breckels, M. N., Brooks, I. M., Browse, J., Burrows,
904 S. M., Carslaw, K. S., Huffman, J. A., Judd, C., Kilhau, W. P., Mason, R. H., McFiggans, G.,
905 Miller, L. A., Nájera, J. J., Polishchuk, E., Rae, S., Schiller, C. L., Si, M., Vergara-Temprado, J.,
906 Whale, T. F., Wong, J. P. S., Wurl, O., Yakobi-Hancock, J. D., Abbatt, J. P. D., Aller, J. Y.,
907 Bertram, A. K., Knopf, D. A., and Murray, B. J.: A marine biogenic source of atmospheric ice-
908 nucleating particles, *Nature*, 525, 234–238, <https://doi.org/10.1038/nature14986>, 2015.
- 909 Wu, M., Liu, X., Yu, H., Wang, H., Shi, Y., Yang, K., Darnenov, A., Wu, C., Wang, Z., Luo, T.,
910 Feng, Y., and Ke, Z.: Understanding processes that control dust spatial distributions with global
911 climate models and satellite observations, *Atmos. Chem. Phys.*, 20, 13835–13855,
912 <https://doi.org/10.5194/acp-20-13835-2020>, 2020.
- 913 Yang, Y., Wang, H., Smith, S. J., Easter, R., Ma, P.-L., Qian, Y., Yu, H., Li, C., and Rasch, P. J.:
914 Global source attribution of sulfate concentration and direct and indirect radiative forcing, *Atmos.*
915 *Chem. Phys.*, 17, 8903–8922, <https://doi.org/10.5194/acp-17-8903-2017>, 2017a.
- 916 Yang, Y., Wang, H., Smith, S. J., Ma, P.-L., and Rasch, P. J.: Source attribution of black carbon
917 and its direct radiative forcing in China, *Atmos. Chem. Phys.*, 17, 4319–4336,
918 <https://doi.org/10.5194/acp-17-4319-2017>, 2017b.
- 919 Yang, Y., Wang, H., Smith, S. J., Zhang, R., Lou, S., Yu, H., Li, C., and Rasch, P. J.: Source
920 Apportionments of Aerosols and Their Direct Radiative Forcing and Long-Term Trends Over
921 Continental United States, *Earth's Future*, 6, 793–808, <https://doi.org/10.1029/2018EF000859>,
922 2018.



- 923 Zender, C. S., Bian, H., and Newman, D.: Mineral Dust Entrainment and Deposition (DEAD)
924 model: Description and 1990s dust climatology, *J. Geophys. Res.*, 108, 4416,
925 <https://doi.org/10.1029/2002JD002775>, 2003.
- 926 Zhang, G. J. and McFarlane, N. A.: Sensitivity of climate simulations to the parameterization of
927 cumulus convection in the Canadian climate centre general circulation model, *Atmos.-Ocean*, 33,
928 407–446, <https://doi.org/10.1080/07055900.1995.9649539>, 1995.
- 929 Zhang, K., Wan, H., Liu, X., Ghan, S. J., Kooperman, G. J., Ma, P.-L., Rasch, P. J., Neubauer,
930 D., and Lohmann, U.: Technical Note: On the use of nudging for aerosol–climate model
931 intercomparison studies, *Atmos. Chem. Phys.*, 14, 8631–8645, <https://doi.org/10.5194/acp-14-8631-2014>, 2014.
- 933 Zhang, M., Liu, X., Diao, M., D’Alessandro, J. J., Wang, Y., Wu, C., Zhang, D., Wang, Z., and
934 Xie, S.: Impacts of representing heterogeneous distribution of cloud liquid and ice on phase
935 partitioning of Arctic mixed-phase clouds with NCAR CAM5, *J. Geophys. Res. Atmos.*, 124,
936 13071–13090, <https://doi.org/10.1029/2019JD030502>, 2019.
- 937 Zhang, M., Xie, S., Liu, X., Lin, W., Zhang, K., Ma, H.-Y., Zheng, X., and Zhang, Y.: Toward
938 understanding the simulated phase partitioning of Arctic single-layer mixed-phase clouds in
939 E3SM, *Earth Space Sci.*, 7, e2020EA001125, <https://doi.org/10.1029/2020EA001125>, 2020.
- 940 Zhang, Y., Xie, S., Lin, W., Klein, S. A., Zelinka, M., Ma, P., Rasch, P. J., Qian, Y., Tang, Q.,
941 and Ma, H.: Evaluation of clouds in version 1 of the E3SM atmosphere model with satellite
942 simulators, *J. Adv. Model. Earth Syst.*, 11, 1253–1268, <https://doi.org/10.1029/2018MS001562>,
943 2019.
- 944 Zhao, X. and Liu, X.: Global Importance of Secondary Ice Production, *Geophys. Res. Lett.*, 48,
945 e2021GL092581, <https://doi.org/10.1029/2021GL092581>, 2021.
- 946 Zhao, X., Liu, X., Burrows, S. M., and Shi, Y.: Effects of marine organic aerosols as sources of
947 immersion-mode ice-nucleating particles on high-latitude mixed-phase clouds, *Atmos. Chem.*
948 *Phys.*, 21, 2305–2327, <https://doi.org/10.5194/acp-21-2305-2021>, 2021a.
- 949 Zhao, X., Liu, X., Phillips, V. T. J., and Patade, S.: Impacts of secondary ice production on
950 Arctic mixed-phase clouds based on ARM observations and CAM6 single-column model
951 simulations, *Atmos. Chem. Phys.*, 21, 5685–5703, <https://doi.org/10.5194/acp-21-5685-2021>,
952 2021b.
- 953



954 **Table 1.** Experiments conducted in this study.

Experiment	Description
CTRL	Control simulation using the CNT parameterization for heterogeneous ice nucleation and Kok et al. (2014a, b) for dust emission parameterization.
noArc	Same as CTRL, but turn off heterogeneous ice nucleation in mixed-phase clouds by HLD.
noNAf	Same as CTRL, but turn off heterogeneous ice nucleation in mixed-phase clouds by North African dust.
noEAs	Same as CTRL, but turn off heterogeneous ice nucleation in mixed-phase clouds by East Asian dust.

955



956 **Table 2.** Annual and seasonal mean Arctic dust burden (mg m^{-2}) from different sources. The
957 numbers in parentheses are the relative contributions (%) of each source to the total Arctic dust
958 burden. The total Arctic dust burden is shown in the last row.

	ANN	MAM	JJA	SON	DJF
Arc	2.1 (30.7)	0.3 (3.9)	5.1 (50.4)	2.5 (47.5)	0.5 (14.6)
NAm	0.1 (0.9)	0.1 (1.3)	0.1 (0.6)	0.0 (0.7)	0.0 (1.2)
NAf	1.7 (24.2)	3.7 (41.4)	1.5 (14.4)	0.7 (12.9)	0.9 (26.4)
CAs	0.9 (12.8)	1.1 (12.5)	1.3 (13.0)	0.8 (14.7)	0.3 (10.1)
MSA	0.8 (11.5)	1.6 (17.9)	0.7 (7.0)	0.3 (6.1)	0.6 (17.4)
EAs	1.4 (19.9)	2.0 (23.0)	1.5 (14.7)	0.9 (18.1)	1.0 (30.2)
RoW	0.0 (0.0)	0.0 (0.0)	0.0 (0.0)	0.0 (0.0)	0.0 (0.1)
Total Burden (mg m^{-2})	6.9	8.9	10.2	5.2	3.3

959



960 **Table 3.** Summary of the nine Arctic INP measurements used for INP comparisons in Figure 8.

	Location	Time	Measured platform	Reference	Possible INP source mentioned in literature	INP source attribution from modeling ⁺
A	Utqiagvik	Spring, 2008	Aircraft	McFarquhar et al. (2011)	Metallic or composed of dust [*]	HLD (NCa) and LLD (EAs)
B	Alert	Spring, 2014	Ground-based	Mason et al. (2016)	Not mentioned	LLD (EAs)
C	Alert	Spring, 2016	Ground-based	Si et al. (2019)	LLD from Gobi Desert	LLD (EAs)
D	Zeppelin	Spring, 2017	Ground-based	Tobo et al. (2019)	Marine organic aerosols	HLD (NEu)
E	Oliktok Point	Spring, 2017	Ground-based	Creamean et al. (2018)	Dust and primary marine aerosols	LLD (mainly from EAs and some from Naf)
F	Alert	Summer, 2014	Ground-based	Mason et al. (2016)	Not mentioned	HLD (NCa)
G	Zeppelin	Summer, 2016	Ground-based	Tobo et al. (2019)	HLD from Svalbard or other high latitude sources ^{**}	HLD (NEu)
H	Utqiagvik	Autumn, 2004	Aircraft	Prenni et al. (2007)	Dust and carbonaceous particles	HLD (NCa) and LLD (EAs)
I	South of Iceland	Autumn, 2014	Aircraft	Sanchez-Marroquin et al. (2020)	Icelandic dust	Dominated by HLD (GrI), little from LLD (Naf)

961 ^{*} Carbonate, black carbon, and organic may also contribute, according to Hiranuma et al. (2013).

962 ^{**} The HLD in this campaign is reported to have remarkably high ice nucleating ability, which
 963 may be related to the presence of organic matter.

964 ⁺ The modeling analyses include INP contribution from HLD, LLD, BC, and SSA.

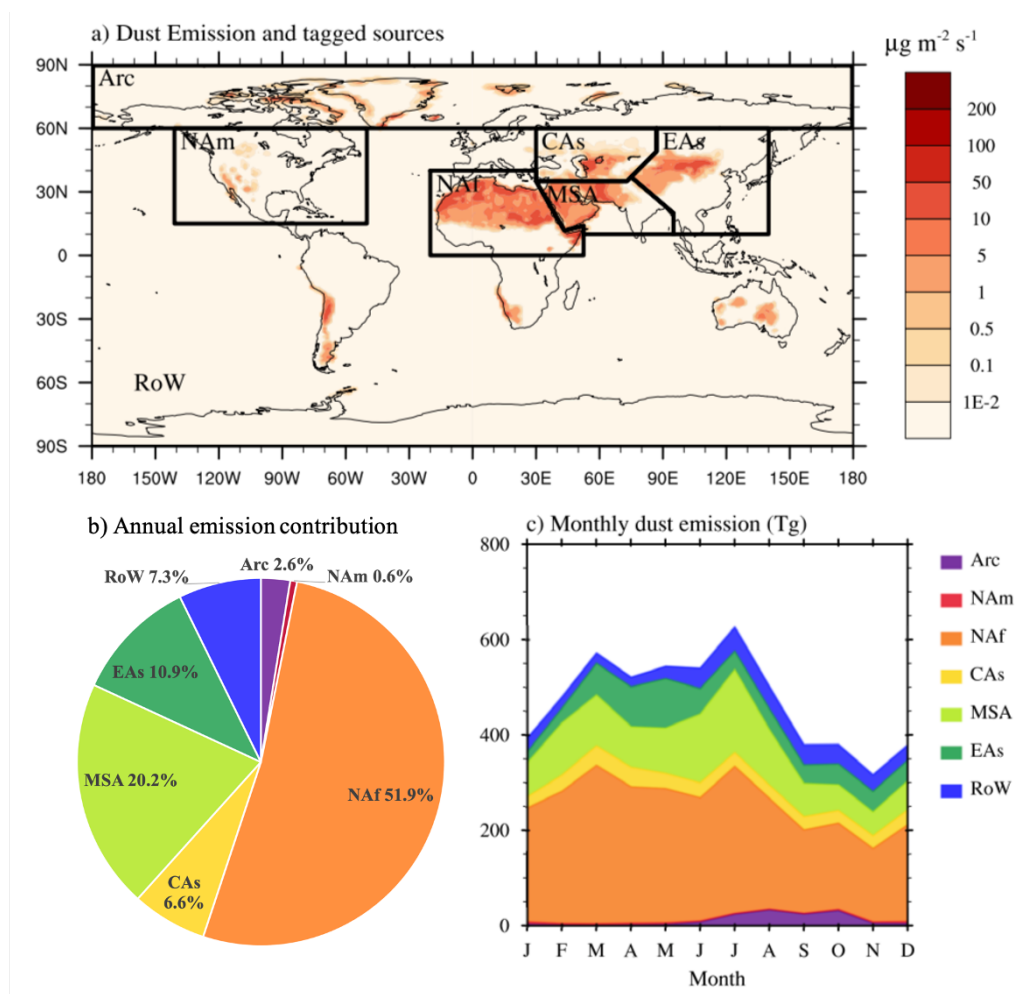
965



966 **Table 4.** Arctic averaged surface downwelling radiative fluxes and TOA cloud radiative forcing
 967 changes caused by dust INPs originated from local Arctic sources (Arc), North Africa (NAf), and
 968 East Asia (EAs). Units are W m^{-2} .

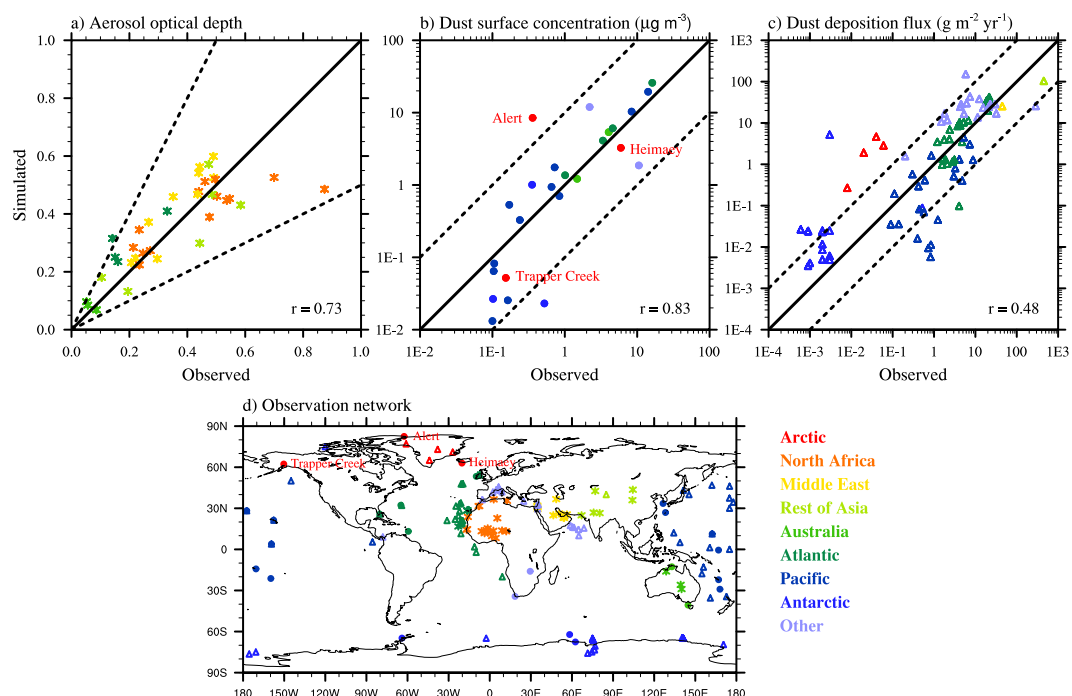
	ANN			MAM			JJA			SON			DJF		
	SW	LW	Net	SW	LW	Net	SW	LW	Net	SW	LW	Net	SW	LW	Net
Part 1. INP effect on surface downwelling radiative fluxes															
Arc	0.11	-0.36	-0.24	0.27	-0.31	-0.03	0.12	0	0.12	0.04	-0.55	-0.51	0.02	-0.56	-0.54
NAf	0.33	-0.25	0.08	0.78	-0.60	0.19	0.50	0.01	0.51	0.02	-0.03	-0.02	0.03	-0.39	-0.36
EAs	0.35	-0.41	-0.06	0.68	-0.60	0.09	0.59	0.02	0.61	0.08	-0.27	-0.19	0.04	-0.80	-0.76
Part 2. INP effect on TOA cloud radiative forcing															
Arc	0.06	-0.11	-0.05	0.06	-0.07	-0.01	0.14	-0.02	0.12	0.03	-0.23	-0.20	0.01	-0.12	-0.11
NAf	0.20	-0.23	-0.03	0.34	-0.34	0	0.41	-0.18	0.24	0.03	-0.20	-0.16	0.02	-0.23	-0.21
EAs	0.20	-0.24	-0.04	0.22	-0.23	-0.02	0.46	-0.17	0.29	0.09	-0.29	-0.20	0.02	-0.26	-0.24

969



970

971 **Figure 1.** a) Simulated global annual mean dust emission with 7 tagged source regions (Arc:
972 Arctic; NAm: North America; NAf: North Africa; CAs: Central Asia; MSA: Middle East and
973 South Asia; EAs: East Asia; RoW: Rest of the World). b) The respective percentage
974 contributions to the global annual mean dust emission from the individual source regions. c)
975 Seasonal cycle of global dust emission.

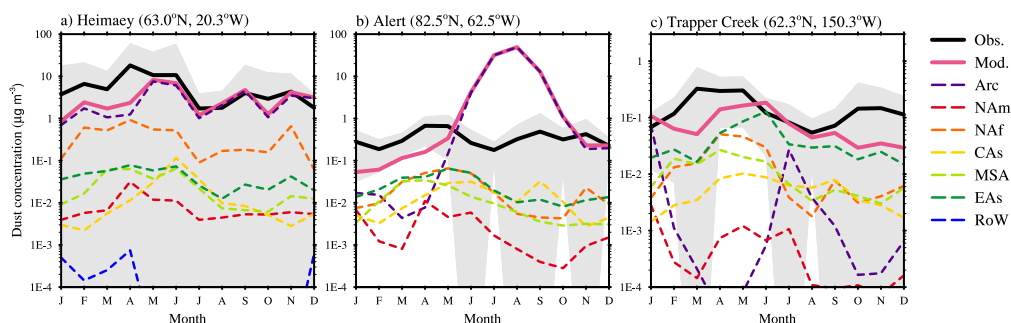


976

977 **Figure 2.** Comparison of observed and simulated a) averaged AOD at 40 dust-dominated
978 stations (stars), b) dust surface concentration at 25 sites (circles), and c) dust deposition flux at
979 84 sites (triangles). Solid lines represent 1:1 comparison. Dashed lines mark 2 factor of
980 magnitude bias in panel a) and 1 order of magnitude differences in panel b) and c). For each
981 comparison, the correlation coefficient (r) is noted. The AOD data is conducted by AERONET.
982 The dust surface concentration measurements include 20 stations managed by Rosenstiel School
983 of Marine and Atmospheric Science at the University of Miami (Prospero et al., 1989; Prospero,
984 1996; Arimoto et al., 1995), two Australia stations (Maenhaut et al., 2000a, b), and three Arctic
985 stations (Heimaey (Prospero et al., 2012), Alert (Fan, 2013), and Trapper Creek (IMPROVE)).
986 The deposition fluxes data is a compilation of measurements from Ginoux et al. (2001),
987 Mahowald et al. (2009), and the Dust Indicators and Records in Terrestrial and Marine
988 Paleoenvironments (DIRTMAP) database (Tegen et al., 2002; Kohfeld and Harrison, 2001).



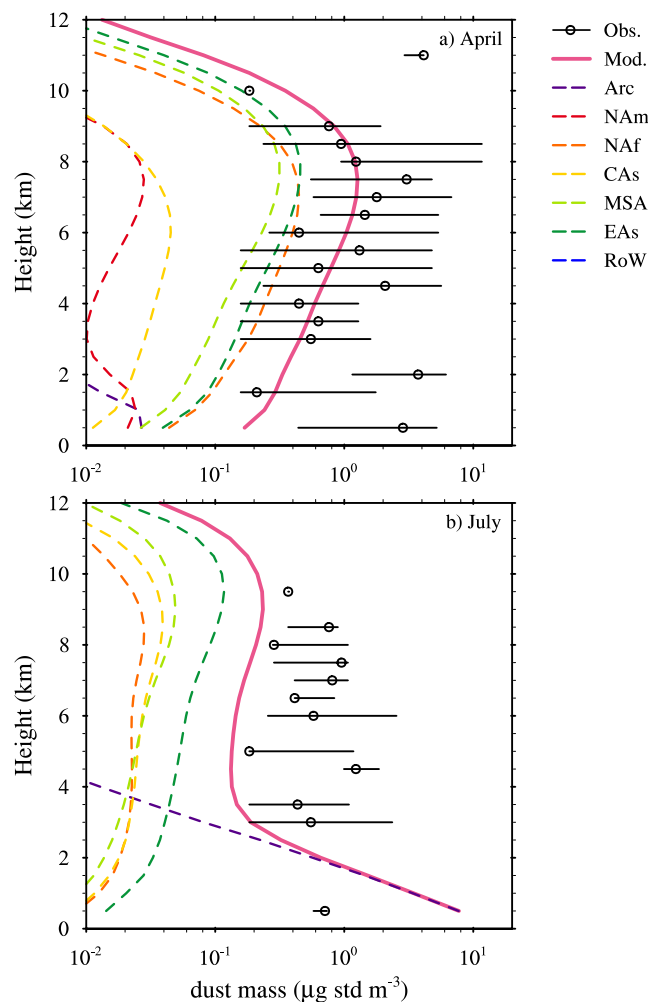
989 Stations are grouped regionally and classified by different colors. The locations of the
990 measurements are shown in panel d).
991



992

993 **Figure 3.** Comparison of measured (black solid line) and simulated (pink solid line) monthly
994 mean dust surface concentration at three high latitude stations – a) Heimaey, b) Alert, and c)
995 Trapper Creek. Contributions from seven tagged sources are shown by colored dashed lines. The
996 locations of the three stations are shown in Figure 2d. The dust concentrations at Trapper Creek
997 only include particles with diameter less than 2.5 μm . The other two stations include dust over
998 the whole size range.

999

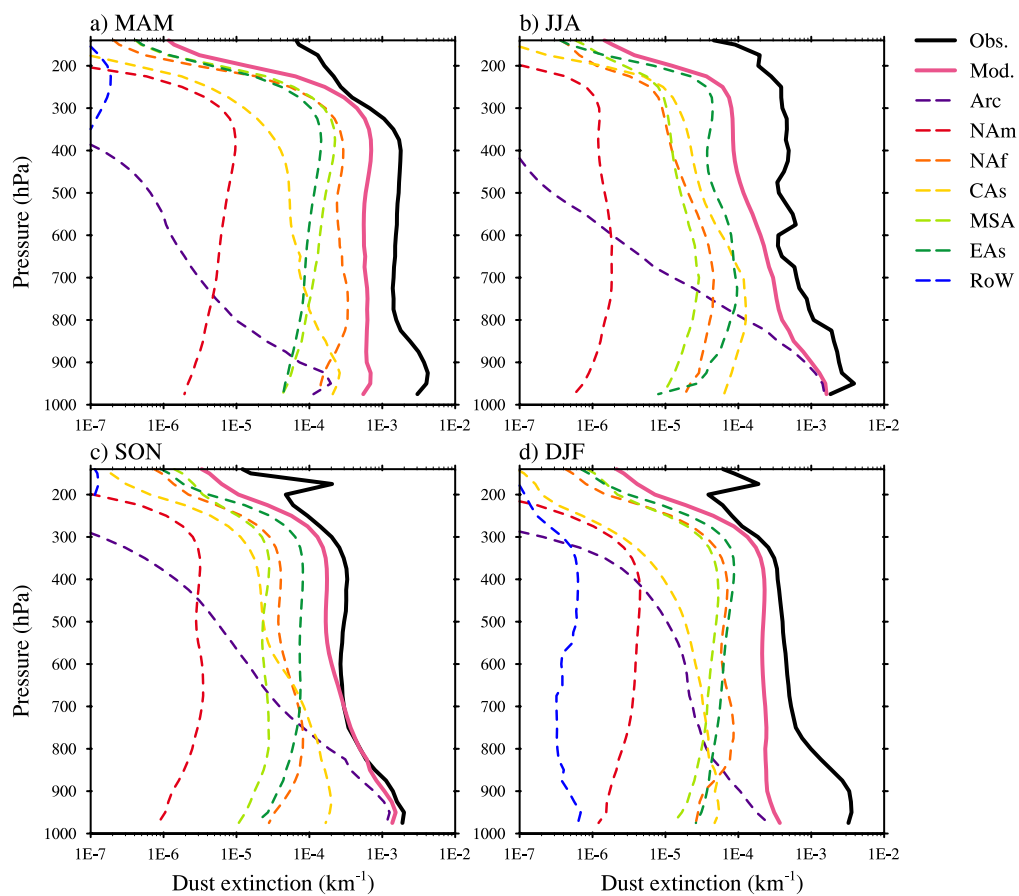


1000

1001 **Figure 4.** Comparison of vertical dust concentrations from ARCTAS flight observations (Jacob
1002 et al., 2010) (black circle) and CTRL simulation (pink solid line) in a) April and b) July. We
1003 show median values for observations at each level. The maximum and minimum of the
1004 measurements at each level are shown by black lines. Contributions from the seven tagged
1005 sources in CTRL are shown by colored dashed lines. The ARCTAS dust mass concentrations are
1006 derived from measured calcium and sodium concentrations. The measurements data are
1007 processed using the same method as Breider et al. (2020). Briefly, we assume a calcium to dust

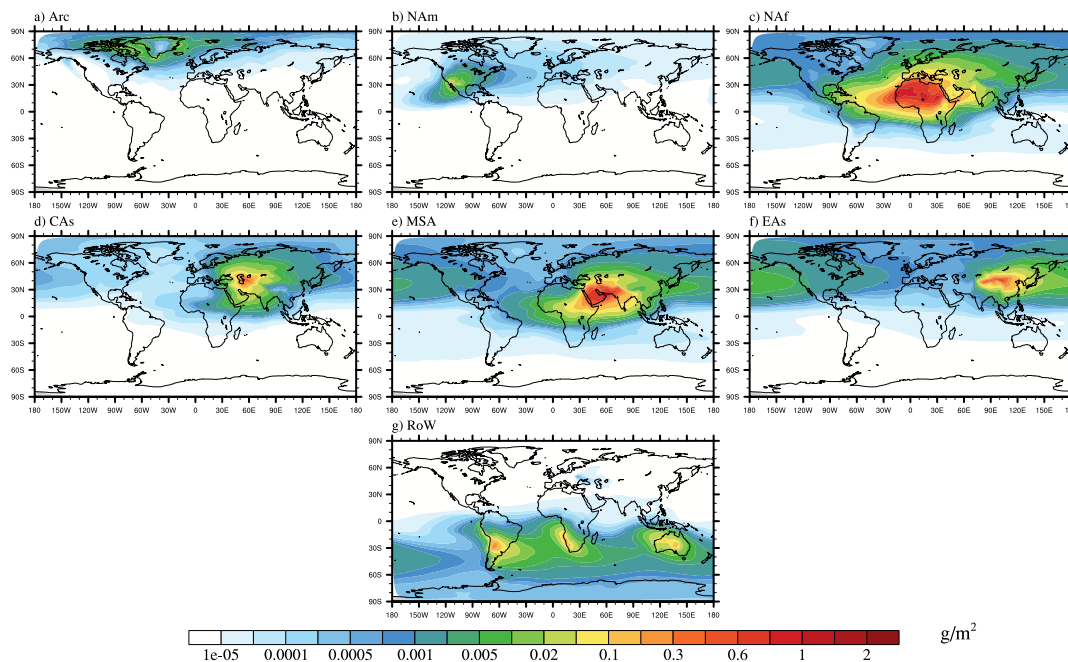


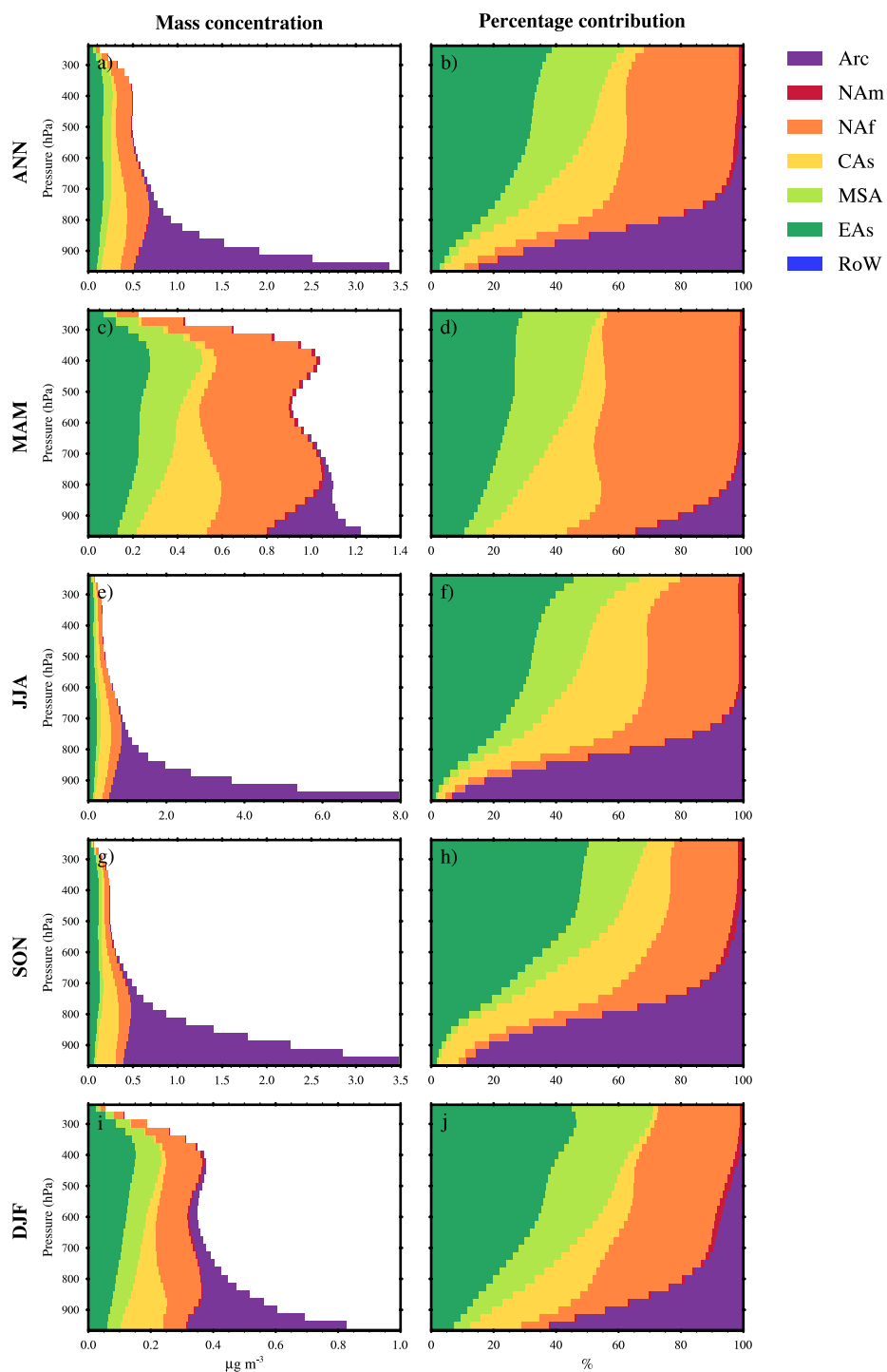
1008 mass ratio of 6.8% and further correct the calcium concentrations for sea salt by assuming a
1009 calcium to sodium ratio of 4%. Only measurements obtained north of 60°N are used for the
1010 analyses. The low-altitude observations near Fairbanks, Barrow, and Prudhoe Bay are removed.
1011 Also, data from below 1 km on 1, 4, 5, 9 July is removed to exclude the influence of wildfire.
1012 The ARCTAS flight campaign was conducted in 2008, while the modeled vertical profiles are
1013 averaged for each April and July from 2007 to 2011, respectively. Following Groot Zwaaftink et
1014 al. (2016), the simulation profiles are averaged for the regions north of 60°N and 170°W to
1015 35°W in April and 135°W to 35°W in July.
1016



1017

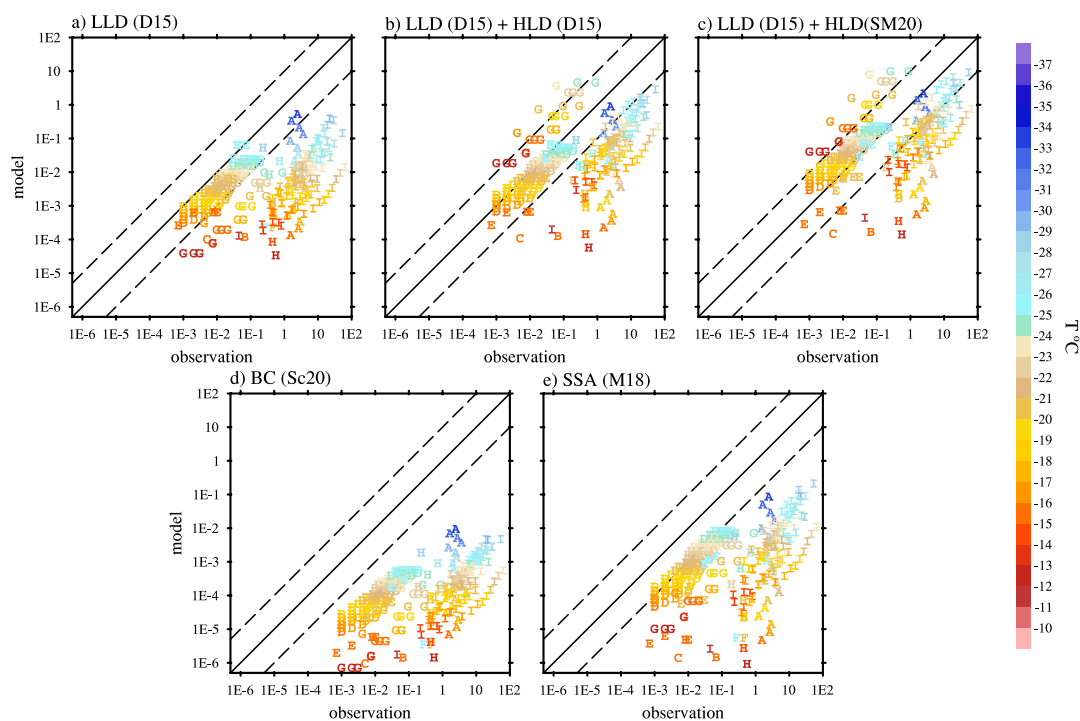
1018 **Figure 5.** Comparison of seasonal CALIPSO retrieved (Luo et al., 2015a, b) (black solid line)
1019 and model simulated (pink solid line) dust extinction vertical profiles in the Arctic. Contributions
1020 from seven tagged sources are shown by colored dashed lines.







1024 **Figure 7.** Annual and seasonal mean Arctic vertical dust concentrations (left panel) and
1025 percentage contributions from tagged sources (right panel). Different tagged sources are
1026 classified by different colors.

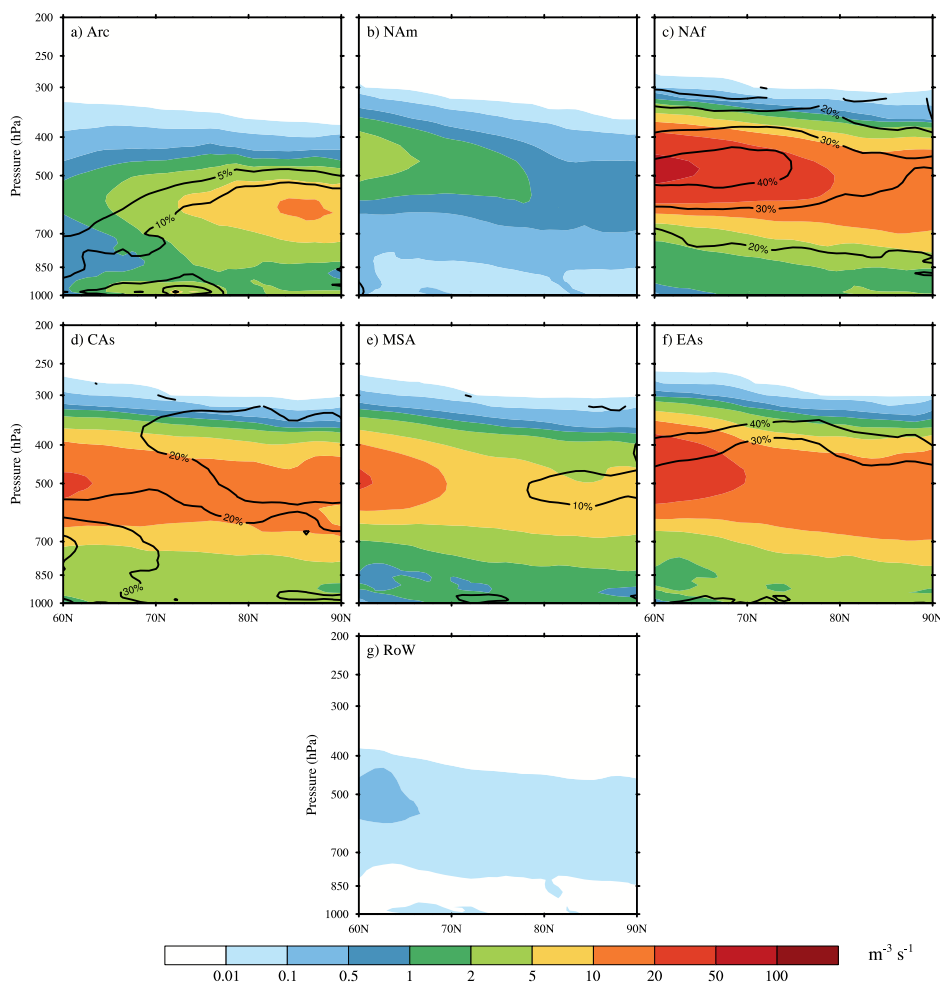


- | | | |
|----------------------------|--------------------------------|-----------------------------------|
| A Utqiagvik (Spring, 2008) | B Alert (Spring, 2014) | C Alert (Spring, 2016) |
| D Zeppelin (Spring, 2017) | E Oliktok Point (Spring, 2017) | F Alert (Summer, 2014) |
| G Zeppelin (Summer, 2016) | H Utqiagvik (Autumn, 2004) | I South of Iceland (Autumn, 2014) |

1027

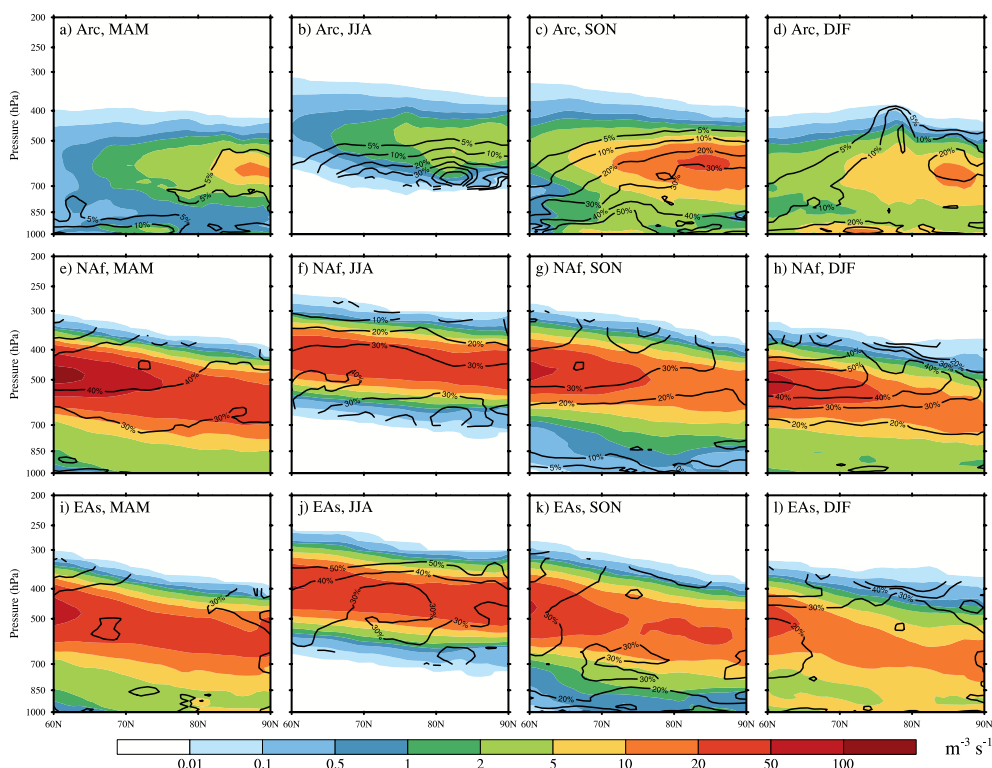
1028 **Figure 8.** Comparison of predicted versus observed INP concentrations in the Arctic. The
 1029 predicted INP concentrations are derived from a) LLD using DeMott et al. (2015; D15), b) LLD
 1030 and HLD, both using D15, c) LLD using D15 and HLD using Sanchez-Marroquin et al (2020;
 1031 SM20), d) BC using Schill et al. (2020; Sc20), and e) SSA using McCluskey et al. (2018; M18).
 1032 SSA includes both marine organic aerosol and sea salt. Nine INP datasets are classified by
 1033 symbol “A” to “I”, the color of which represents the observed temperature. Details of each
 1034 campaign are summarized in Table 3. Solid line in each panel represents 1:1 comparison, while
 1035 dashed lines outline one order of magnitude differences. The unit for INP concentration is L^{-1} .

1036



1037

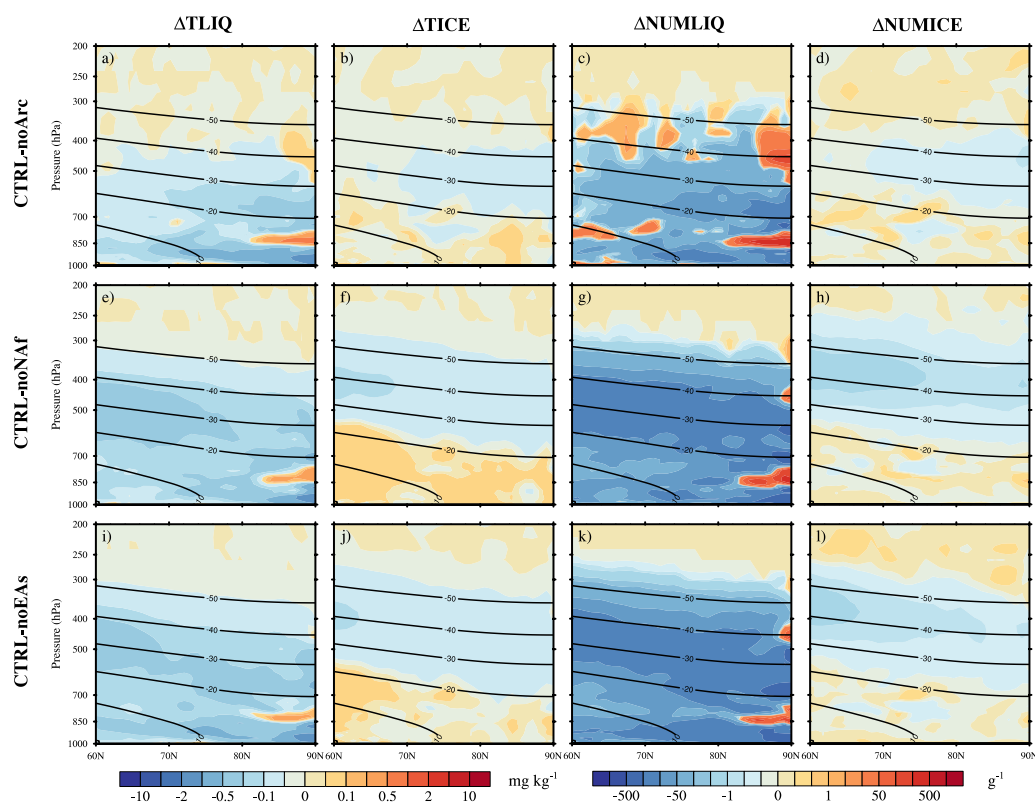
1038 **Figure 9.** Annual and zonal mean ambient mixed-phase cloud immersion freezing rates (unit: m⁻³ s⁻¹) in the Arctic (60-90°N) for the seven dust sources. Black contours are the percentage
1039 ³ s⁻¹) in the Arctic (60-90°N) for the seven dust sources. Black contours are the percentage
1040 contributions from each dust source to the total immersion freezing rate.



1041

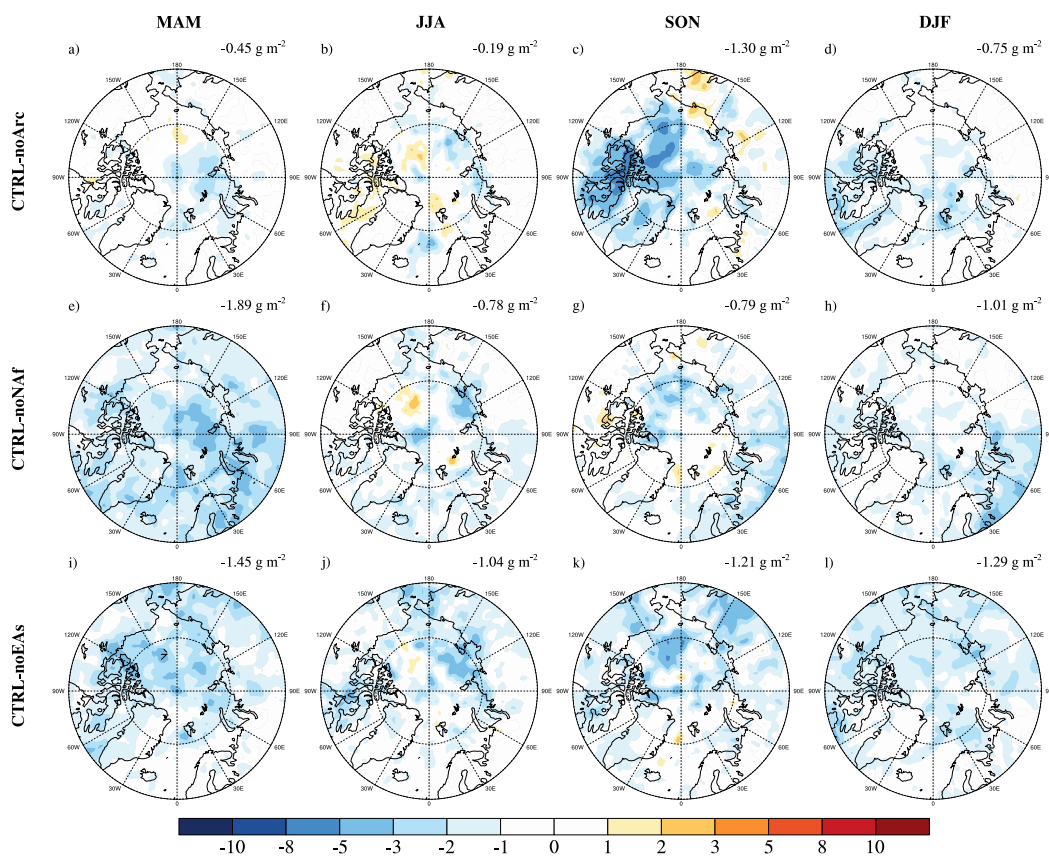
1042 **Figure 10.** Seasonal variations of the mixed-phase clouds immersion freezing rates (unit: $\text{m}^{-3} \text{s}^{-1}$)
1043 over the Arctic for dust emitted from the Arctic (top panel), North Africa (middle panel), and
1044 East Asia (bottom panel). Black contours are the percentage contributions from each dust source
1045 to the total immersion freezing rate in the corresponding season.

1046



1047

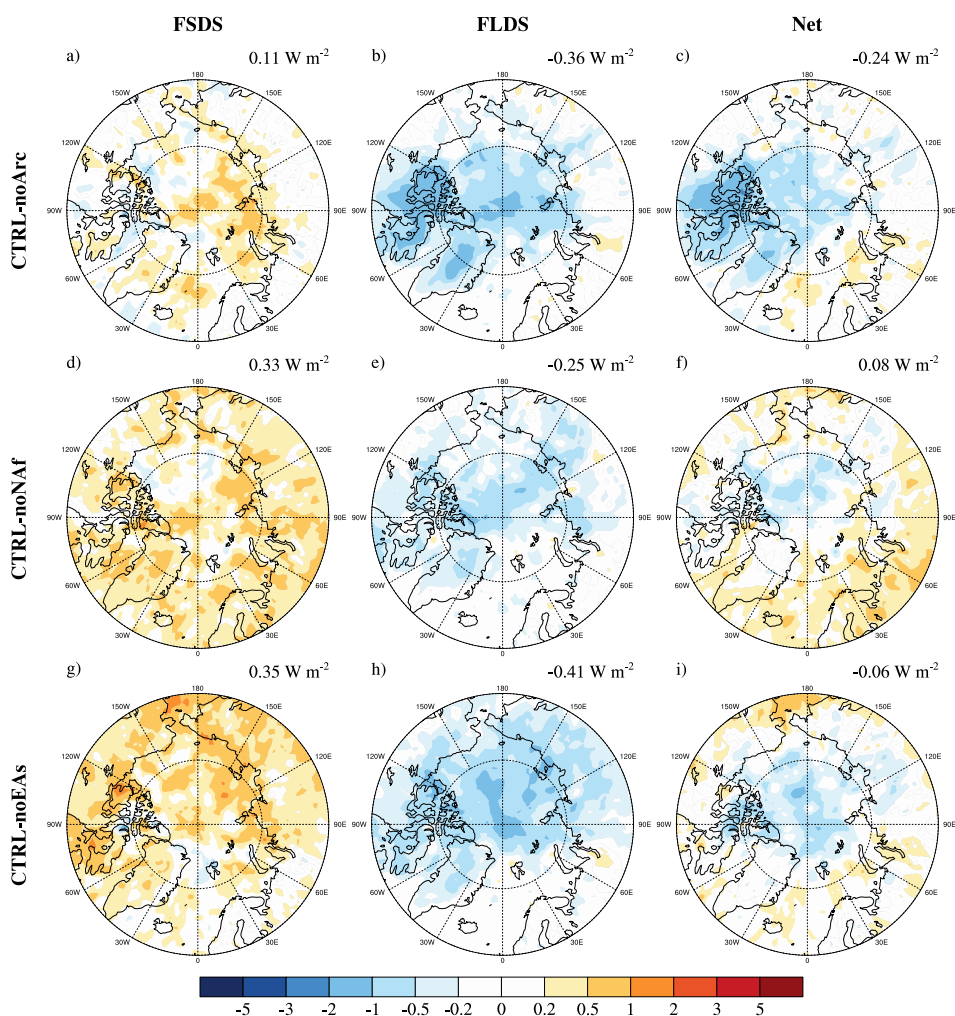
1048 **Figure 11.** Annual and zonal mean differences in total liquid water mass mixing ratio (TLIQ),
1049 total ice mixing ratio (TICE), cloud droplet number concentration (NUMLIQ), and cloud ice
1050 number concentration (NUMICE) in the Arctic. Black contours are zonal averaged temperatures
1051 in °C. Top, middle, and bottom panels show the differences between CTRL and noArc, noNAF,
1052 and noEAs, respectively.



1053

1054 **Figure 12.** Seasonal changes in LWP (unit: g m^{-2}) caused by dust INPs from the Arctic (top
1055 panel), North Africa (middle panel), and East Asia (bottom panel). The numbers are averaged
1056 LWP differences in the Arctic.

1057



1058

1059 **Figure 13.** Changes in annual mean downwelling radiative fluxes at the surface (unit: W m^{-2})
1060 caused by dust INPs from the Arctic (top panel), North Africa (middle panel), and East Asia
1061 (bottom panel). Left, middle, and right panels are downwelling shortwave (FSDS), longwave
1062 (FLDS), and net (FSDS + FLDS) radiative fluxes, respectively. The numbers are averaged
1063 radiative flux differences in the Arctic.